Cold Climate Engineering

MSc Thesis in Cold Climate Engineering

Detection and characterization of icebergs in Kongsfjorden (Svalbard) based on ground-based radar images and additional remote sensing data

Stefan Linge
s181205 | 663803

Supervisors

Henning Skriver
Henriette Skourup
Miina A. Rautiainen
Tom Rune Lauknes
Line Rouyet

DTU

A!

Submitted
28th June 2019

Preface

This thesis is the result of cooperation between the Danish Technical University (DTU), Copenhagen, Denmark, Aalto University, Espoo, Finland, and the NORCE Norwegian Research Centre, Tromsø, Norway. The thesis has been completed at NORCE and marks the final qualification in the Cold Climate Engineering programme. Prof. Henning Skriver (DTU), Prof. Henriette Skourup (DTU), Prof. Miina A. Rautiainen (Aalto), Senior Researcher Tom Rune Lauknes (NORCE) and Researcher / PhD Student Line Rouyet (NORCE) form the thesis supervisory team. This thesis reflects five months of work and results in 30 ECTS credits. All work is my own.

In order to evaluate the capabilities of a ground-based radar system for the detection of icebergs in Kongsfjorden, the thesis takes advantage of the images acquired during the project Remote Sensing of fjord ICe and effects on Ecosystems (RESICE) led by NORCE and funded by Arctic 2030 Programme (Ministry of Climate and Environment, Ministry of Foreign Affairs, Norway).

Abstract

This thesis focuses on the exploitation of ground-based radar images to detect icebergs. Additional remote sensing data from space-borne Synthetic Aperture Radar (SAR), Unmanned Aerial Vehicle (UAV) and in-situ boat tracks has been used to compare and validate the results. The investigation site is located in Kongsfjorden (Svalbard) and the combined data acquisition took place during a two-week campaign in April 2018. Five tidewater glaciers terminate in Kongsfjorden and produce a large number of icebergs of different sizes and shapes. The ground-based radar had an elevated position in Ny-Ålesund to overview a several kilometer-wide section of the fjord. The ground-based radar used during the campaign is the GAMMA Portable Radar Interferometer (GPRI). The 5 min temporal resolution of the dataset allows one to make comparisons with the above mentioned auxiliary remote sensing data. The software Python was used to process the GPRI data.

Firstly, the GPRI images were pre-processed to account for the decreasing performance in range resolution. Secondly, an area of interest located between Ny-Ålesund and Blomstrandhalvøya was chosen. Hereby, it is important to focus only on the sea region and to leave out lagoons and other coastal lines. The area of interest covers approximately 2 km long region with only water and icebergs passing by while leaving Kongsfjorden. Thirdly, a threshold was applied to the GPRI images in order to separate potential icebergs from the sea background. Analysing histograms of both iceberg and sea background is important to find the appropriate threshold. This makes sure to include as many true positive as possible. In general, we can choose between two threshold modes, namely the automated and the manual threshold methods. The automated threshold method relies on the 99.93^{th} percentile and shows the best compromise between all GPRI images. The automated threshold method is efficient and preferably used for big amounts of data and small time slots, because one loses small icebergs or detect false alarms. Therefore, it is more effective to decide on the manual threshold method. It is time-consuming, but one can more easily distinguish between iceberg and sea background by adjusting the threshold manually. Fourthly, in order to document important parameters based on GPRI images, we extract the count, size and position of every detected iceberg. Finally, the resulting GPRI images can be georeferenced and compared with auxiliary data. The software QGIS is a useful tool to compare the GPRI image products with satellite SAR images, drone images and boat tracks. After evaluating the GPRI images with auxiliary data, it turned out that the number of detected icebergs can be increased by choosing the manual threshold method, since the positive alarms are the majority in comparison to false alarms.

For the future, the automated version could be improved by applying an advanced target detection, which is already used in synthetic aperture radar imagery. The developed algorithm for iceberg detection could be further developed to track. The GPRI's temporal resolution of 5 min is predestined for such a tracking system, because it is easier to separate different icebergs within a shorter time frame. The potential value of the results can not be overseen in terms of climate research. In the future, scientists can build upon the findings to determine the mass balance of tidewater glaciers by observing how much calved ice is leaving the fjord system. In addition, the ground-based radar is showing a high potential in detecting icebergs, even if those are rather small. This could provide new insights on the distribution, volumetry and motion of icebergs, valuable for documenting oceanic currents.

Acknowledgement

I would like to thank Prof. Henning Skriver, Prof. Henriette Skourup, at the DTU, and Prof. Miina A. Rautiainen, at Aalto, my thesis supervisors, for their patient guidance and useful critiques of this work. Thanks to Tom Rune Lauknes, my supervisor at NORCE, for all the support and guidance when processing GPRI data. Heidi Hindberg at NORCE, your contribution to this project has been invaluable and I appreciate all the knowledge I learned from you about Python (I hope my thousand questions weren't too annoying). The door to Tom Grydeland (NORCE) was always open whenever I ran into trouble and thank you for always taking time to teach me new gdar or Python tricks. A special thanks to Jakob, Jörg, Ståle, Temesgen, Tenaw, Fabio, Barbro, Rannveig, Agnar, Markus and all the wonderful people at NORCE for making my project as comfortable as possible. I want to thank NORCE for letting me use their office. Thank you, Siva innovasjonssenter, for offering me your gym.

I must express my gratitude to Line (NORCE) for providing me with continuous encouragement and for her constructive recommendations on this project. Thanks for all the time and effort you have put into assisting me. This wouldn't have been possible without you and your Norut jacket.

Magnus, Esme, Jana, Matěj, Can, Daniel and Silvi from kitchen uno, thank you for being such an awesome company throughout my stay in Tromsø. I'll never forget our (not so) deep conversations, karaoke nights and the Game of Thrones marathon.

Mama, Papa, Schwestl and Omi, thank you for your constant support and love during my Scandinavian adventure.

… Opa. I know you would have been proud.

Stefan Linge – June 2019, Tromsø

Table of Contents

List of Figures

List of Tables

1 Introduction

This thesis is about detection of icebergs using GAMMA Portable Radar Interferometer (GPRI) images. In this chapter we present the motivation and the structure of the thesis.

1.1 Motivation

The Arctic and Antarctica regions, in particular where ocean and coastal areas interact, mark an important interface of various processes. Here, Cryosphere, Hydrosphere and Biosphere are forming a complex mesh of interactions that can affect every human being in the long term. On the one hand, the rapidly changing climate is strongly influencing the Arctic regions. On the other hand, that Arctic transformation is going to influence the ecosystem of the rest of the Earth. In general, increasing warmth is abetting the melting of glaciers. The glacier mass loss from calving may increase and thus it may have an impact on the freshwater flux. It is of high importance that we focus on investigating these floating bits and the consequences for the ecosystem [1][2][3].

Icebergs and growlers are a risk to ships and offshore structures alike in the high Arctic. Fishing industry, oil and gas companies, transport infrastructure and the tourism branch are immediate affected by the changing climate. It would be beneficial to make conclusions about the dynamics of icebergs and the total mass of ice the fjord contributes to the Arctic sea, which is only possible with long and continuous observations. In future studies, these new insights might be key information to develop more precise models related to the climate. Even in immediate time frames, the ground-based radar system could be used as an early-warning system to inform nearby vessels of potential threats – namely floating icebergs. It also underlines the need of an automatic iceberg detection system, which could be provided with the help of the GPRI system. In Kongsfjorden, the five tidewater glaciers, Blomstrandbreen, Conwaybreen, Kongsbreen, Kronebreen and Kongsvegen, are calving the icebergs. To estimate the number of calved icebergs flowing out of the fjord system is a potential contribution to quantify the calving component of the glacier mass loss. Moreover, the thesis could be seen as contribution to modeling of oceanic currents, and prediction of positions to mitigate the risk for shipping [4][5].

Using different remote sensing techniques has several benefits. Not only can we show their capabilities in detecting icebergs but also make a conclusion about choosing the best possible observation technique in the future considering key data properties (e.g. spatial/temporal resolution and coverage). This thesis concentrates on analyzing the GPRI's capabilities in detecting icebergs in Kongsfjorden. The method and results may be helpful for further investigations and applications in oceanography and glaciology in Svalbard, or in similar arctic regions of the Earth.

1.2 Objectives

The main priority of this work is to evaluate the GPRI's capability in detecting icebergs. A threshold has to be applied to the GPRI images in order to separate potential icebergs from the sea. The results of the iceberg detector are compared with auxiliary remote sensing data. We evaluate the iceberg detection performance based on GPRI images with satellite Synthetic Aperture Radar (SAR) images, Unmanned Aerial Vehicle (UAV) imagery and in-situ boat tracks encircling icebergs (figure 1).

It makes it possible to make conclusions about the sensitivity, detection benefits and limits of ground-based radar systems. In addition to the GPRI data, satellite data from RADARSAT-2 and Sentinel-1, UAV images, and boat track information from the Norwegian Polar Institute (NPI) have been used for validation.

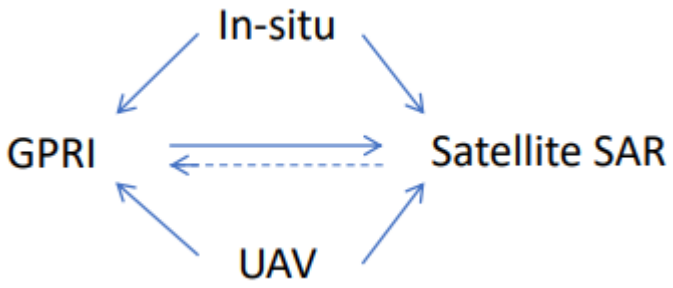

Figure 1: Overview for GPRI data validation with the help of auxiliary data.

After analyzing the GPRI's detection effectiveness, my secondary objective is to gain more information about the detected icebergs. Not only am I interested in the iceberg position, but also I want to know the iceberg parameters count and size. In particular, that should give potential information regarding the ice mass balance in Kongsfjorden.

The following research questions are dedicated to my objectives and shall be answered in the concluding part of this thesis.

1. Is it possible to identify icebergs in Kongsfjorden based on the backscatter intensity of GPRI images?

2. Which threshold technique is the most adapted to the detection of icebergs based on GPRI images?

3. Compared to complementary remote sensing and in-situ data, can we evaluate the quality of the results and identify false positives/negatives?

4. What information, for example count, size or shape of icebergs, can we gain from the GPRI images?

1.3 Related Work

1.3.1 Icebergs and Growlers

The melting season in Kongsfjorden usually starts in June, but warm spells with more than 0 degree Celsius in the spring are not unusual. Kongsfjorden has seasonal fast ice in its inner part. The ice thickness was varying from 0.9 m (1999) to 0.71 m (2005) with its maximum in 2004. The snow layer is on average 0.225 m thick. In addition, the five tidewater glaciers terminating in Kongsfjorden produce calved icebergs floating out of the fjord (figure 2). In general, up to 40% of the calved icebergs floating out of Kongsfjorden have a width of less than 0.5 m. In contrast, only less than 10% are more than 5 m wide. The maximum width observed was 30 m, but such a case is extremely rare. Even more than 20 m width for icebergs can be seen as outlier. When it comes to the freeboard, we can see that up to 80% of the icebergs have a freeboard smaller than 0.5 m. Around 15% of the icebergs have a freeboard higher than 1 m. Outliers are up to 6 m in height. It can be concluded that the size distribution is not constant. Apparently, it exists a temporal variation in the distribution of freeboard sizes. Floating icebergs and growlers are the priority targets for the detection based on radar images, but we need to be aware that seasonal fast ice might also get detected [4][6][7][8].

Figure 2: Floating iceberg in Kongsfjorden (photo taken by Sebastian Gerland April 2018).

1.3.2 Remote Sensing of Icebergs

There has been a numerous amount of remote sensing techniques that can be applied to specific areas of the Cryosphere, like for iceberg detection in the Arctic and Antarctic regions. A significant number of them were using microwave and optical sensors mounted on space- and air-borne vehicles, for example, satellite SAR and cameras on UAV respectively. Radars have the advantage of being used during day and night, and during any kind of weather condition, because they are operating in the Microwave domain. The radar antenna is an active sensor that does not need any other light source, for example the Sun. Furthermore, the electromagnetic waves with Microwave frequencies are capable of penetrating clouds. For SAR remote sensing,

it is important to take the backscatter signal into account. Before receiving any backscatter, the antenna sends out electromagnetic waves. The backscatter signal is the signal received by the antenna when the electromagnetic waves are traveling back. In general, we distinguish between three types of reflection for backscatter signals when we use the GPRI in Kongsfjorden (figure 3). Specular reflections occur when the electromagnetic waves are hitting the sea surface and scatter away from the radar, which is why the GPRI will not receive any signal in return. Diffuse signals are happening when strong sea disturbance occurs, which means that the rough sea surface can reflect some of the electromagnetic waves back to the radar. The GPRI antenna can also receive corner reflections coming from an iceberg in Kongsfjorden. In detail, the backscatter signal and its intensity depend on four main properties: 1) different sizes, shapes and overall structures of the icebergs; 2) the surrounding geophysical properties, for example sea surface properties (roughness and temperature); 3) the sensor properties, for example incidence angle, frequency and polarization; 4) the backscatter coming from nearby targets (for example interferences from buildings) which are not sea or icebergs can influence the measurements. That is why the iceberg detector focuses preferably on an area of interest without lagoon or coast line that can influence the backscatter intensity. Optical sensors, for example RGB cameras, are passive instruments, which means that they need a secondary light source to receive electromagnetic waves in the optical domain (figure 4). Hence, we can only use optical sensors during day time. Satellites with optical sensors cannot take useful images on cloudy days. In comparison, drones are flying at lower altitude and can operate independent from cloud coverage. The most challenging part is to collect the various remote sensing data at the exact time [9][10][11].

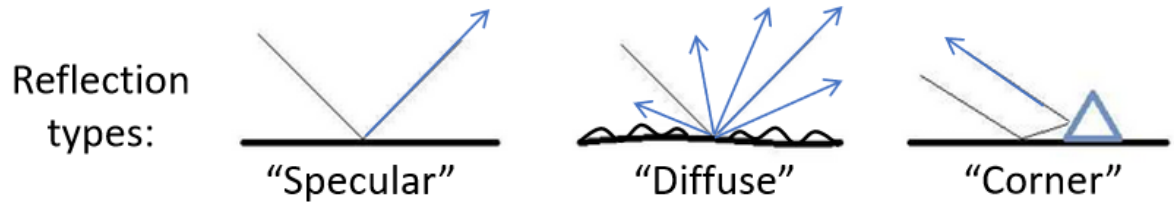

Figure 3: Three reflection types for GPRI backscatter signals in Kongsfjorden.

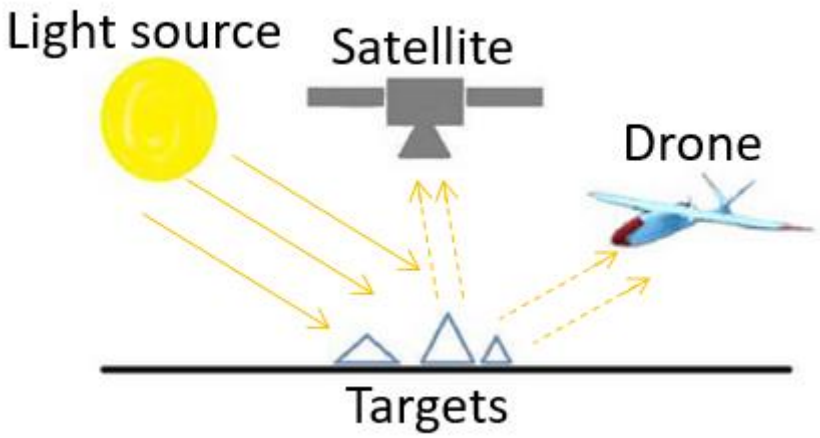

Figure 4: Working principle of passive Earth Observation sensors.

1.3.3 Ground-based Radar for Iceberg Detection

In general, the number of projects using terrestrial radar for iceberg detection or even tracking is relatively sparse. As previously mentioned, the majority of the remote sensing missions observing growlers are based on satellite and drone observations. As an example, for ground-based radar systems, D. Voytenko has been using a GPRI for iceberg detection. From the iceberg positions, he could derive the surface currents within a fjord in southeastern Iceland [12][13].

In this paragraph, I want to show D. Voytenko's example on how he used the GPRI data. His observation took place in Jökulsárlón, which is a proglacial lagoon in Iceland's southeast. The campaign took place in August 2012 for 43.5 h and the GPRI's temporal resolution was 2 min. The basic idea of D. Voytenko's approach is to take images of the backscattered signals and extract out the position of as many icebergs as possible. On the one hand, since the ground-based radar has a low elevation angle and is looking at the fjord, the transmitted signals are reflected by all objects floating in the fjord. On the other hand, the flat-water surface makes sure that incoming radar waves get scattered away from the radar. Therefore, the icebergs are highlighted as strong backscatter in the images. That makes it easy to distinguish between floating bits and water. All the GPRI images have to be converted into maps of certain spacing before starting the processing. The pre-processing of each radar image involves two main steps. Firstly, masking out the lagoon boundary and anything beyond is crucial, because the area of interest is the sea and it simplifies the detection algorithm. Secondly, in order to minimize the unavoidable noise (which is taken as a basis to all radar data), D. Voytenko uses a combination of several Gaussian blurs and thresholds. The resulting maps are a stack of binary images containing the detected growlers (value 1) and the sea (value 2). Some very small icebergs might be lost due to the noise reduction. Due to the natural current within the fjord, the icebergs are in motion. Hence, no image will be the same as its predecessor and successor. The detection algorithm labels every object visible in the first image of the stack and calculates their centroid positions. The centroid positions correspond to the x and y coordinates found in the two-dimensional image. Furthermore, the algorithm compares all the centroid positions with the new ones of the following image. Based on a specified distance, the detector labels a nearby object as the same object from the previous image, or it finds a new object. The idea is to track the object positions in time by using the nearest-neighbor method and create velocity maps to observe the currents within the fjord. The iceberg detection approach is a promising method which can be applied to other GPRI data [12][13].

1.4 Thesis Contents

Chapter 1 focuses on the project's motivation, objectives, and its overall scientific background for remote sensing of icebergs with the help of ground-based radar, satellite SAR and drone instrumentation. Chapter 2 introduces the study area in Kongsfjorden and discusses the above-mentioned datasets, including provided in-situ data. Chapter 3 presents the method for detection of icebergs based on GPRI data. Chapter 4 presents the results of the detection and the validation with auxiliary remote sensing data. Chapter 5 discusses the success of the processing chain and the potential for future work. Chapter 6 concludes this thesis.

2 Study Area and Dataset

2.1 Kongsfjorden Study Area

The GPRI instrument has been used for the data acquisition in Kongsfjorden, a fjord in the western part of Svalbard (figure 5). Kongsfjorden is approx. 25 km long and up to 10 km wide. Located on Spitsbergen's western coast, the most important landmarks are the island Blomstrandhalvøya and five tidewater glaciers. These glaciers, namely Blomstrandbreen, Conwaybreen, Kongsbreen, Kronebreen and Kongsvegen, are producing the icebergs floating in Kongsfjorden. Therefore, Kongsfjorden serves as a big laboratory for a broad range of research disciplines concerning the Arctic ecosystem. The majority of icebergs and fast sea-ice is leaving the fjord between Ny-Ålesund and Blomstrandhalvøya. The GPRI is facing the fjord and its spatial coverage includes the section between both locations. Normally, Kongsfjorden becomes fast-ice-free during the summer season around July. We can expect for Kongsfjorden to contain icebergs and fast-ice during the April campaign [3][7][14].

The coordinates of the GPRI are 78°56'45" N and 11°52'29" E in Ny-Ålesund and close to the shore. It was located on the roof of an abandoned mining factory at 57 m above sea level (figure 6). Hereby, it is very important to take the natural variability of the backscatter signal into account. This variability is happening due to the changing incidence angle when the GPRI is located several meters above sea level. The backscattered signal is changing in intensity because the ground-based radar is looking upon the fjord from a higher position, namely the roof of an old mining building. When we look at such acquisition geometry, there will be additional factors caused by environmental physics that influence the backscatter profile. In particular, random wave patterns, wind and surface currents can cause issues when processing the GPRI images. In addition, interferences from other infrastructure in Ny-Ålesund can occur.

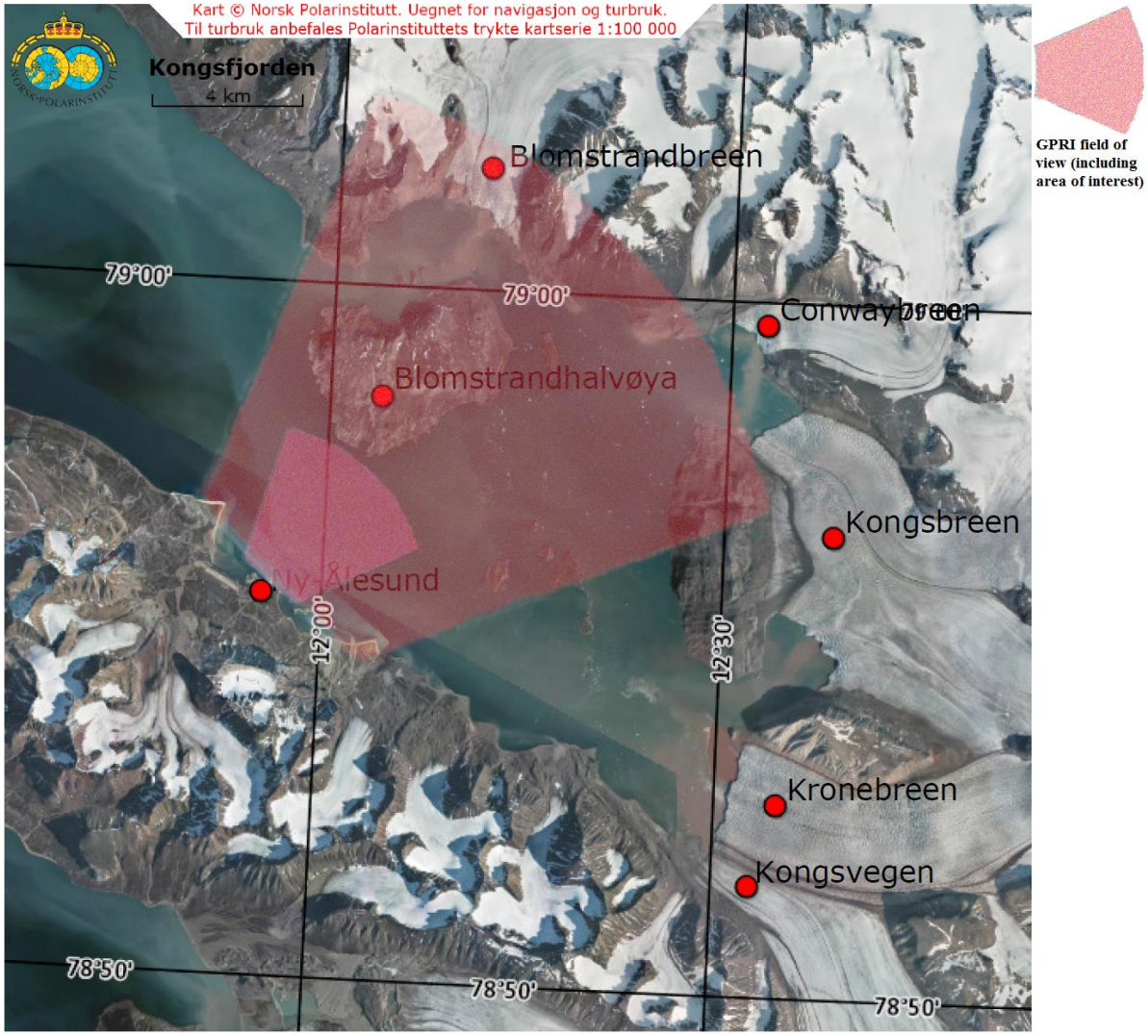

Figure 5: Map of Kongsfjorden in Svalbard (provided by Norwegian Polar Institute https://toposvalbard.npolar.no/). The GPRI was located in Ny-Ålesund and looking at Kongsfjorden.

The GPRI's recording time from February to October 2018 allowed to acquire a large amount of data. The campaign was led by the Earth Observation group of the Norwegian Research Centre NORCE, which is localized in Tromsø. Senior Researcher Dr. Tom Rune Lauknes and Researcher Line Rouyet have been responsible for the set-up and inspection of the GPRI throughout the campaign. Originally, the ground-based radar was developed and built by the GAMMA Remote Sensing AG which is a Swiss company (Aktiengesellschaft – AG). The GPRI was bought and is owned by NORCE. In order to protect the radar equipment, a weatherproof radome was enclosing the GPRI on the roof of an abandoned mining building in Ny-Ålesund (figure 7).

Figure 6: The GPRI's location (red circle) on the roof of an abandoned mining building in Ny-Ålesund (photo taken by Line Rouyet 26.04.2018).

Figure 7: The radome protecting the GPRI facing Kongsfjorden in Ny-Ålesund (photo taken by Line Rouyet 25.04.2018).

2.2 GPRI

The overall GPRI campaign has been conducted in Kongsfjorden from February to October 2018, but I am focusing on the April 2018 part and its joint operations. The temporal resolution of the GPRI during the rest of the acquisition period is 15 min. The 5 min temporal resolution and the complementary data in April 2018 is perfect for the evaluation of the iceberg detector. The Single Looking Complex (.slc) files are the GPRI products that serve as input for the iceberg detection algorithm.

We know from different projects that the GPRI is popular to detect and measure surface displacements, for example in mountainous areas based on the phase component [15]. However, the iceberg detector is based on the work of the amplitude component of the .slc images. The GPRI which acquired the raw data is using real-aperture antennas. In detail, one antenna is transmitting and the two remaining antennas are receiving microwave radiation (figure 8). The reason why the antenna system rotates in azimuth direction is to build up the images line by line. Basically, the radar system is operating at 17.2 GHz, which belongs to the Ku-band domain. The GPRI's most important parameters relevant to this thesis are presented in Table 1 [16].

Figure 8: GPRI system without radome (photo taken by Line Rouyet).

Table 1: GPRI data properties.

GPRI data properties	
Acquisition period	16.04. – 26.04.2018
Data type	Single Look Complex (.slc) image
Size of imaged area	approx. 154 km^2
View angle	170°
Frequency / wavelength	17.2 GHz / 0.017 m
Temporal resolution	5 min
Spatial resolution	in range: constant 0.75 m in azimuth: linear decrease with distance ➔ approx. 7 m at 1 km ➔ approx. 14 m at 2 km etc.

During the two-week campaign from 16.04. to 26.04.2018, the GPRI was acquiring data every five minutes. Due to its high temporal resolution, it can give valuable information on the iceberg positions, and provide statistics about their number and size. The azimuth spatial resolution becomes worse linearly with increasing range, for example it is about 21 m at 3 km (figure 9). The decreasing spatial resolution is further illustrated in figure 10, for example an iceberg would appear larger at range 2 in comparison to another iceberg at range 1 [17][18].

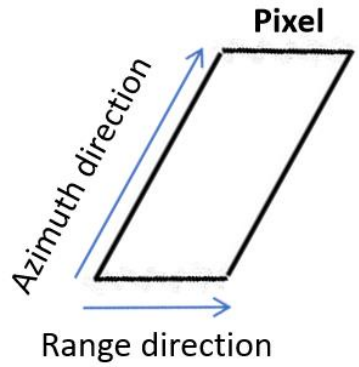

Figure 9: Pixel geometry.

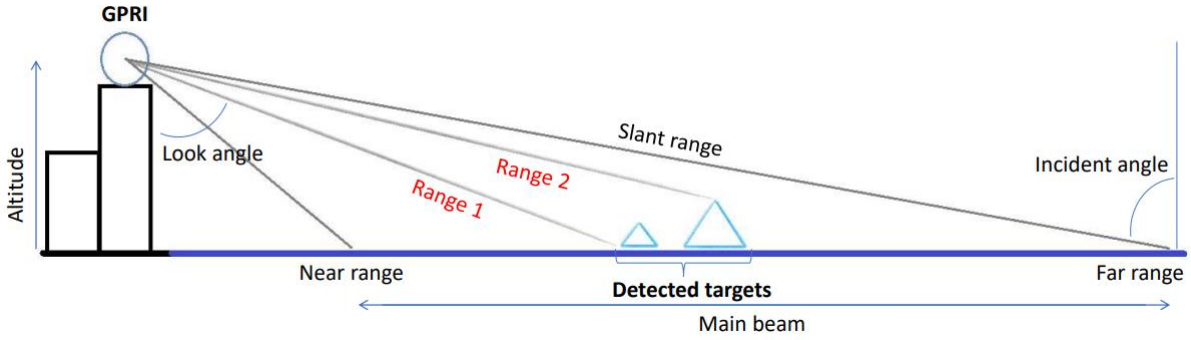

Figure 10: GPRI geometry set up.

2.3 Satellite SAR

Synthetic Aperture Radar (SAR) is a widely used sensor on board of Earth Observation satellites. As the name suggests, its remote sensing instrument of choice is the radar operating in the Microwave domain. In comparison to a real aperture antenna, the SAR satellite creates its own long antenna synthetically while flying over the area of interest. Basically, the longer the antenna, the finer is the resolution of the resulting image. Hereby, SAR satellites play an important role in observing the Earth with a high resolution [19].

SAR satellite systems have several advantages over most of the optical passive instruments. Where optical passive instruments are limited to day time and the weather, radar instruments can operate no matter what time it is and the condition on the ground. SAR is sending actively microwave radiation down to the Earth's surface and collects all backscattered signals coming back to the antenna. This active mode of transmitting and receiving microwave radiation of a certain wavelength makes the SAR satellite independent of Sun illumination. Furthermore, the electromagnetic waves in the microwave domain can penetrate clouds, which often is a limiting factor for passive instruments like optical cameras mounted on satellites. If we look at terrestrial radars, we see that space-borne SAR satellites are not limited to only one area of interest. Basically, every SAR satellite covers almost the entire Earth, where ground-based radars cannot cover large areas within minutes. We can see that flying and stationary radars serve different purposes. The SAR satellite covers large areas for the cost of low temporal

resolution, because the satellite needs several days to come back to the same location it is interested in, whereas the ground-based radar can investigate its area of interest continuously with a high resolution. Usually, one more major drawback of the SAR satellite is its lower resolution in comparison to terrestrial systems in the near-range. In the far-range, the GPRI has a poor resolution of for example approx. 70 m at 10 km [20].

Two well-known SAR satellite programmes are Sentinel-1 and Radarsat-2. Sentinel-1 belongs to the Copernicus programme of the European Space Agency (ESA) and Radarsat-2 is a Canadian Space Agency mission. Both, Sentinel-1 satellites and Radarsat-2 have an operational frequency of 5.405 GHz, which is the C-band domain. Radarsat-2 needs 24 days to pass over the same area of interest again. Since the Sentinel-1 mission involves two satellites, namely Sentinel-1A and Sentinel-1B, it has a shorter repeat cycle. Usually, one satellite alone needs 12 days, but Sentinel-1A and Sentinel-1B share the same orbit 180° apart. This results in a repeat interval of 6 days. Figure 11 shows the different operation modes that are used by ESA's Sentinel-1 satellites. Radarsat-2 is using similar acquisition modes. The following overview focuses on the main differences of both satellite SAR systems (table 2). Sentinel-1 used Interferometric Wide Swath (IWS) and Extra Wide Swath (EWS), and Radarsat-2 used Fine Quad-Pol [21].

Table 2: Satellite SAR properties.

	Sentinel-1	**Radarsat-2**
Operation mode(s)	IWS / EWS	Fine Quad-Pol
Spatial resolution (rg x az)	~ 5x20 m / ~ 20x40 m	~ 11x9 m
Revisit time (temporal resolution)	12 (6) days	24 days
Polarization	Dual-polarimetric	Quad-polarimetric
Data products	.slc	.slc

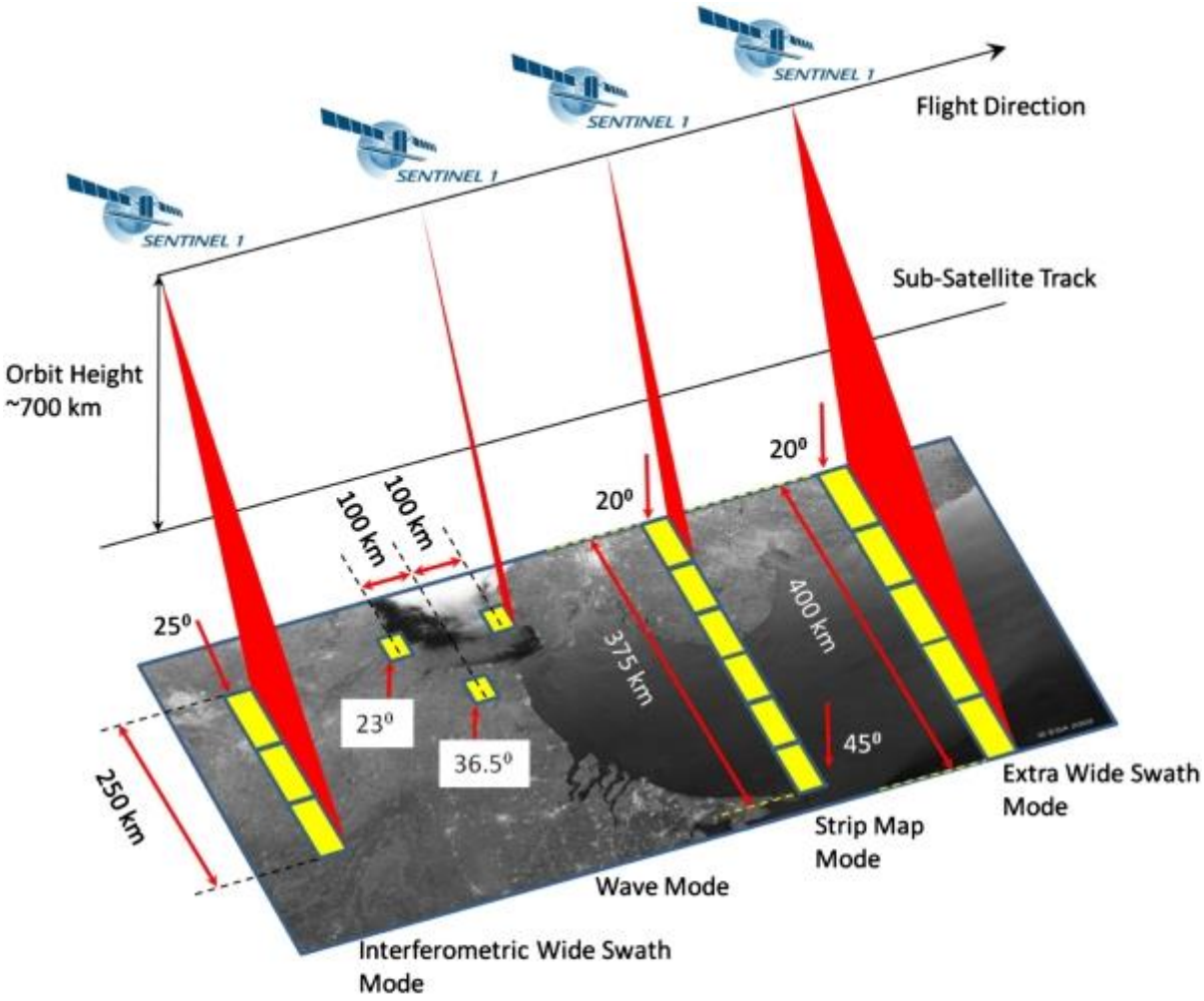

Figure 11: Acquisition modes used by ESA's Sentinel 1 satellite (image taken from https://sentinel.esa.int/web/sentinel/user-guides/sentinel-1-sar/acquisition-modes).

2.4 UAV

The Drone flights were prepared, coordinated and executed by the Drone Technology group at NORCE, Tromsø. The drone is called CryoWing Scout UAV and has a cruise speed of 22 m/s (figure 12). Included in the 11 kg takeoff weight, it has the FLIR PtGrey Chameleon 2, which is an RGB camera with 5 Mpix and a focal length of 12.5 mm. The camera offers a sufficient quality to evaluate the optical images in terms of iceberg detection [22].

Figure 12: The CryoWing Scout UAV located in Ny-Ålesund (photo taken by Agnar H. Sivertsen April 2018).

Every user can browse on the platform http://nlive.norut.no/nlive/#guest=1 called Norut Live Map (NLive) web service, operated by the Drone Technology group at NORCE. The example image shows an optical image taken by the camera mounted on the drone (figure 13). The drone was located near the lagoon of Blomstrandhalvøya and could take an image of an iceberg. Anyhow, the large georeferenced drone data set makes it possible to find iceberg images in order to validate the GPRI images (figure 14).

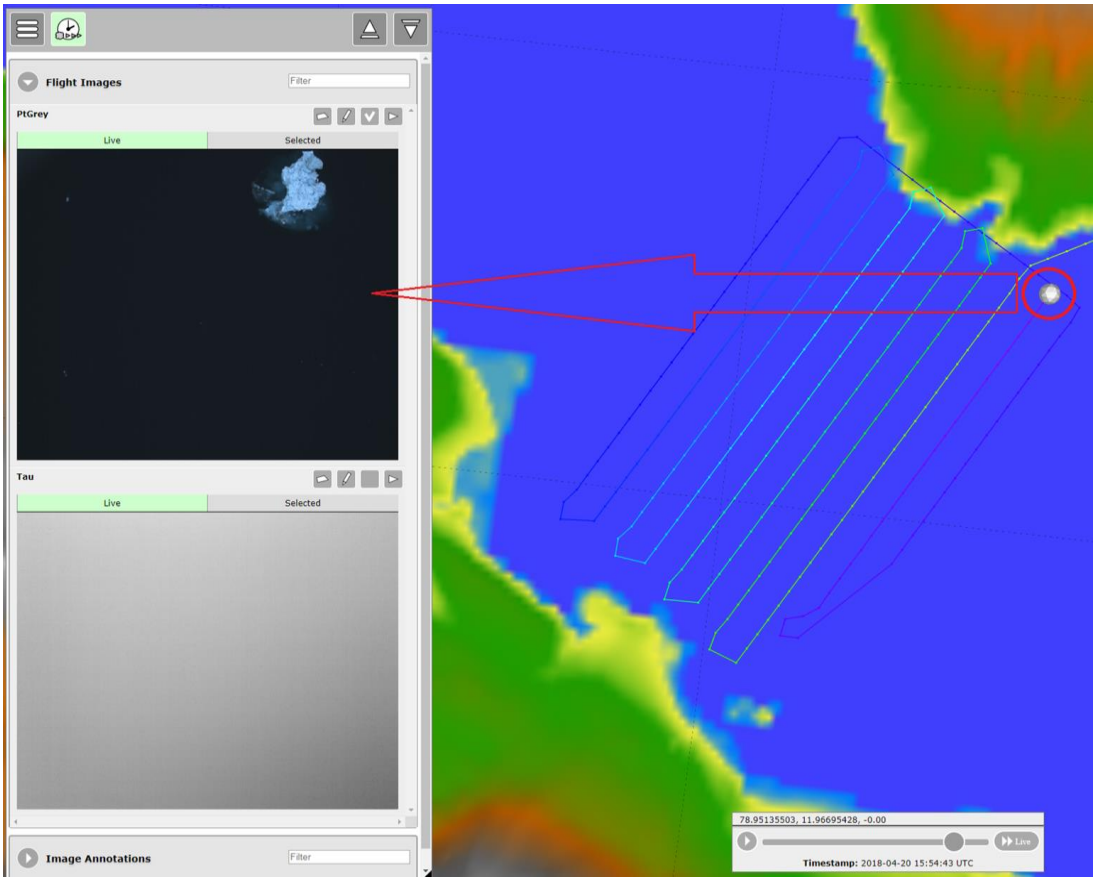

Figure 13: NLive web service example image from 20.04.2018 at 15:54:43 UTC.

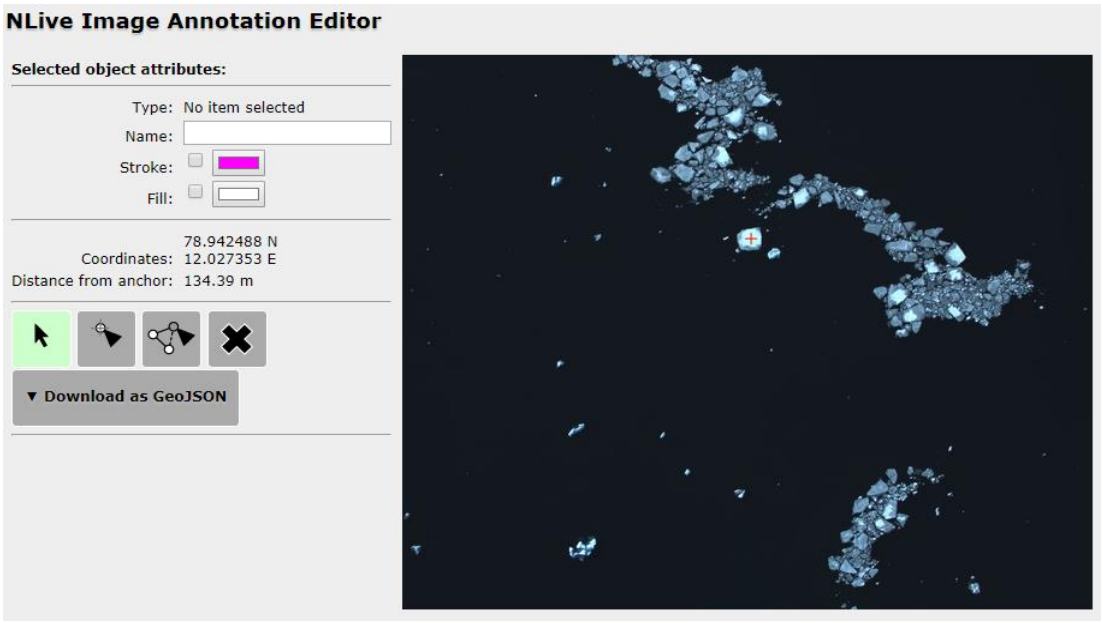

Figure 14: The NLive Image Annotation Editor allows the user to find the location of each iceberg.

2.5 In-situ measurements

The in-situ measurement campaign in April 2018 was conducted by the Norwegian Polar Institute (NPI). It consists of many different measurements focusing on characterizing the sea ice and the icebergs. For the evaluation of the GPRI's iceberg detection capabilities, the GPS boat tracks are of particular interest. During the NPI boat trips into Kongsfjorden, the boat was surrounding floating icebergs. Figure 15 shows an example of an iceberg circumnavigated by NPI. It is possible to validate some of the detected icebergs with the GPS data the NPI boat was taking. In addition to the tracks, the NPI researchers were taking pictures of every encircled iceberg, which is helpful to illustrate how the icebergs looked like on the field. The boat tracks can be mapped in QGIS (figure 16).

Figure 15: Circumnavigated iceberg (photo taken by Sebastian Gerland April 2018).

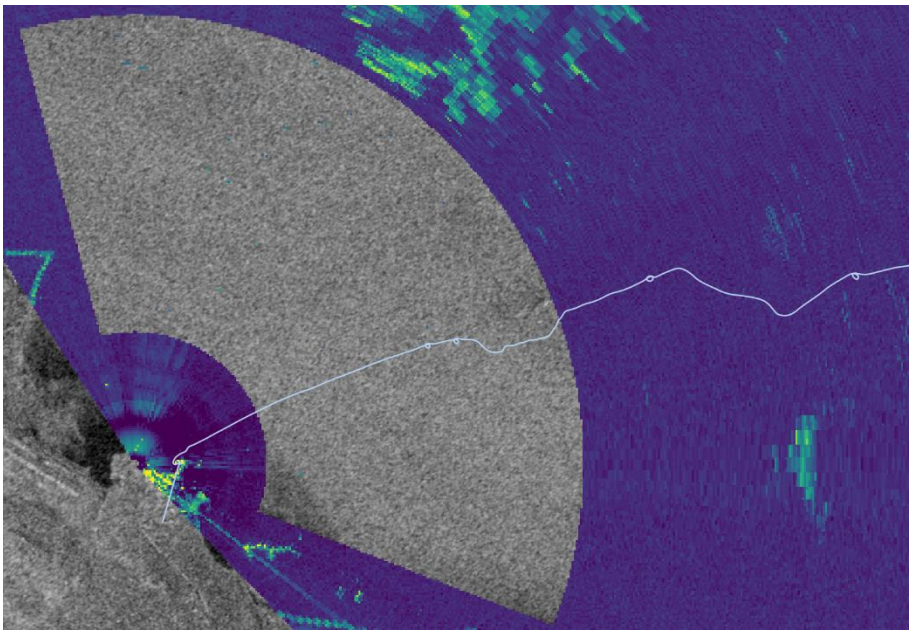

Figure 16: NPI boat track within the GPRI backscatter image.

3 Methodology

3.1 Detection of Icebergs

The following detection mechanism for all the GPRI images is created with the help of the programming language Python. Further, the coding part can be found in the appendix of this contribution. Furthermore, I added comment lines to make the code easier to understand.

The following overview shows the idea of how to detect icebergs with the help of the GPRI and auxiliary data (figure 17). Firstly, the GPRI image has to be read in order to enable the further processing. Secondly, the GPRI image has to be corrected for the variability of the backscatter signal in range direction. Thirdly, after the preprocessing, the GPRI image can be processed. Fourthly, we can visualize our results by georeferencing the GPRI backscatter image. Fifthly, we extract the iceberg parameters position, count and size of all detected icebergs from the GPRI image. Finally, we are using auxiliary data, for example satellite SAR images, to validate the georeferenced GPRI image.

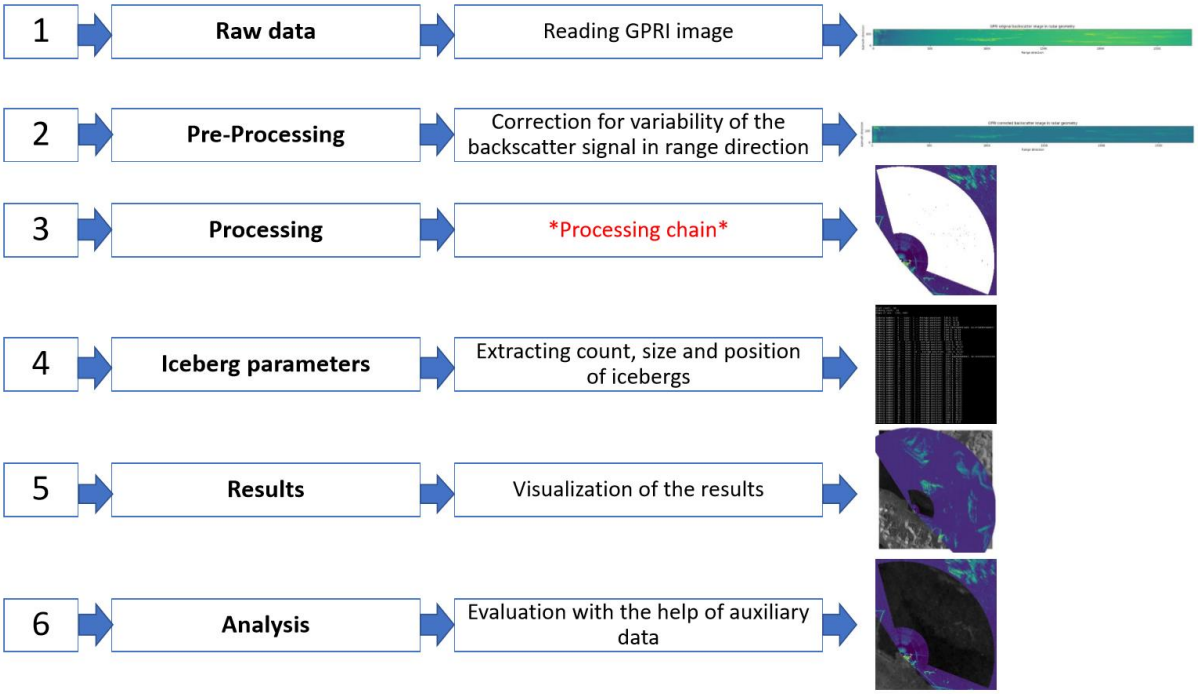

Figure 17: Detection of icebergs overview.

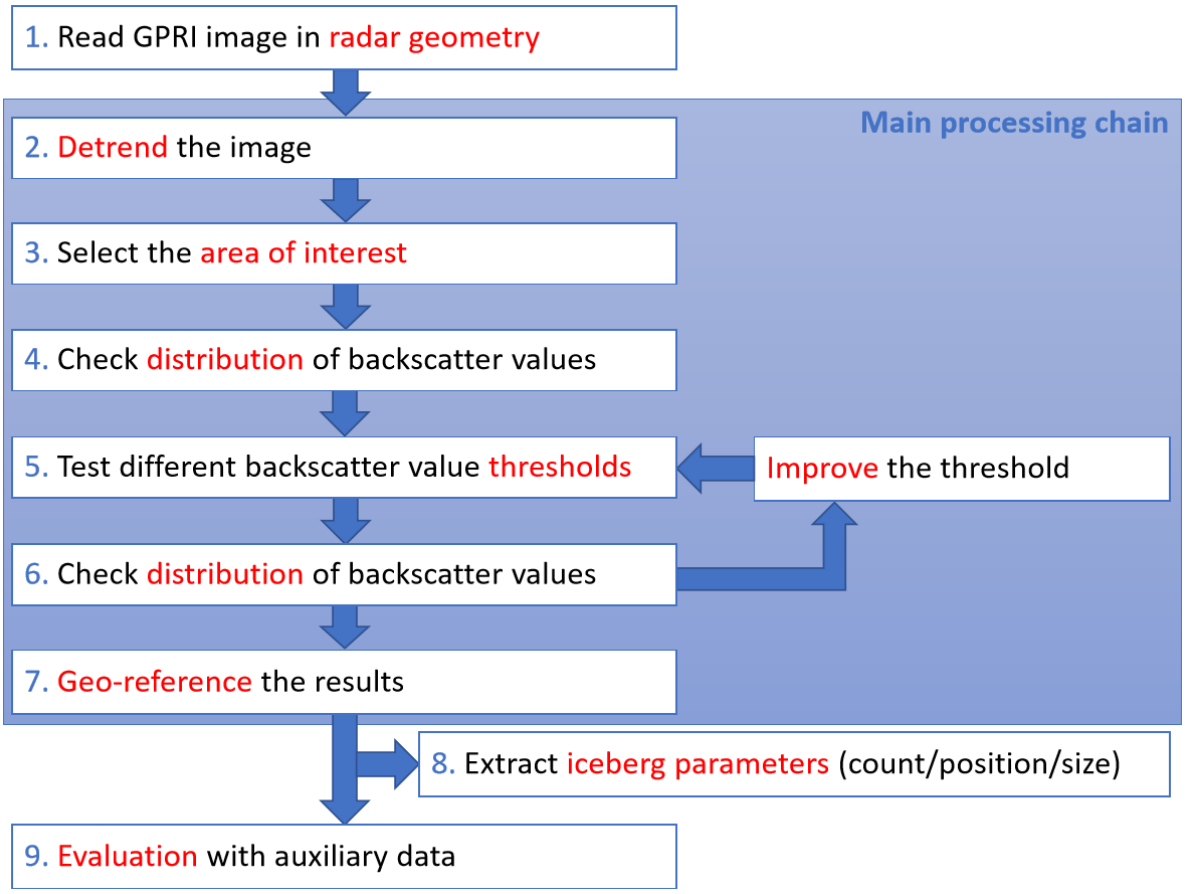

Figure 18: Processing chain in detail.

The main processing chain is illustrated in figure 18. We are using one example GPRI backscatter image to present the processing steps. The GPRI backscatter image was acquired on the 24th of April 2018 at 15:50:01 UTC.

3.2 Processing Steps

In step 1, we read the backscatter intensity component of the SLC images (figure 19). The GPRI backscatter image is shown in radar geometry, which contains azimuth and range direction. Figure 20 is focusing on the area of interest in the GPRI backscatter image. In order to make it easier to understand, we can plot the GPRI backscatter intensity image in a polar coordinate system (figure 21). We can also zoom to the area of interest in polar coordinates of our GPRI backscatter intensity image (figure 22). Figure 19 and 21 make a trend in range direction visible. The backscatter intensity values in the GPRI image are changing with increasing range due to change of incidence angle. In order to extract the variability of the backscatter intensity in range direction, we have to detrend the GPRI backscatter image. If a threshold is applied to the unprocessed GPRI backscatter intensity image, we would have decreasing detection performance with increasing range. This can cause uncertainties, for example in choosing an optimal threshold to separate potential icebergs from the background.

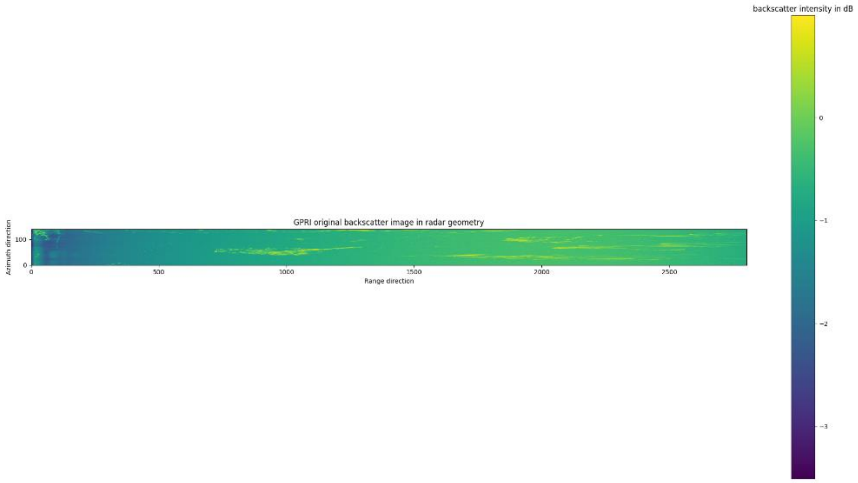

Figure 19: GPRI backscatter image in radar geometry without processing (from 24.04.2018 15:50:01).

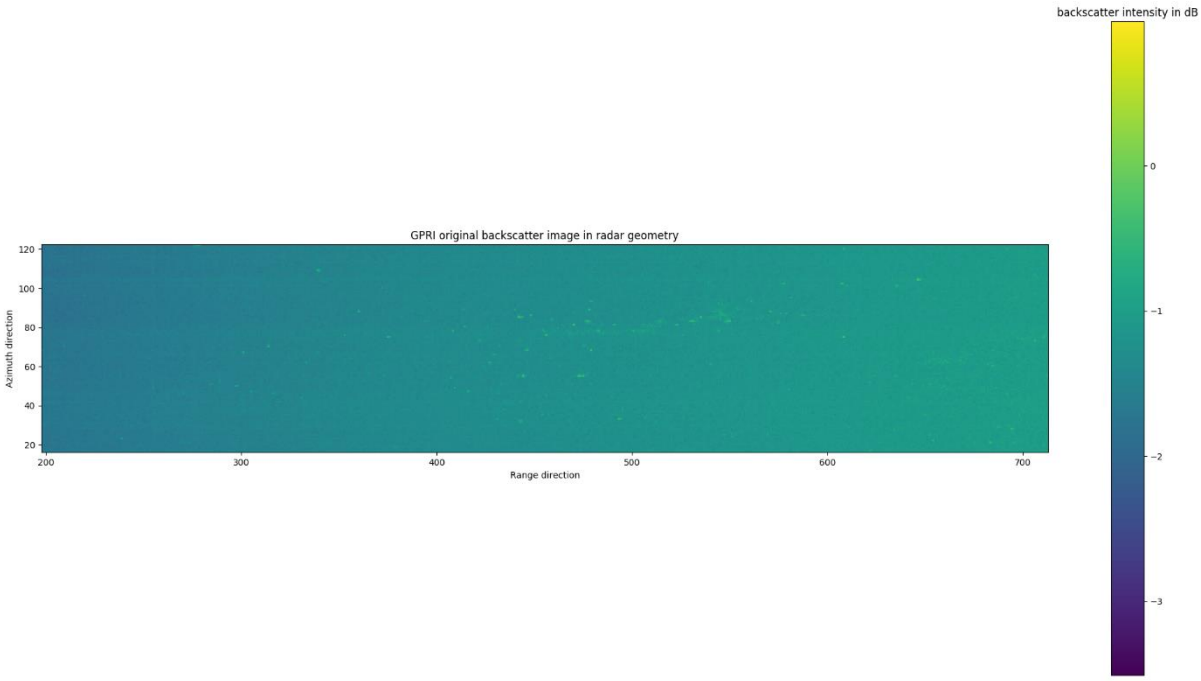

Figure 20: GPRI backscatter image at area of interest in radar geometry without processing (from 24.04.2018 15:50:01).

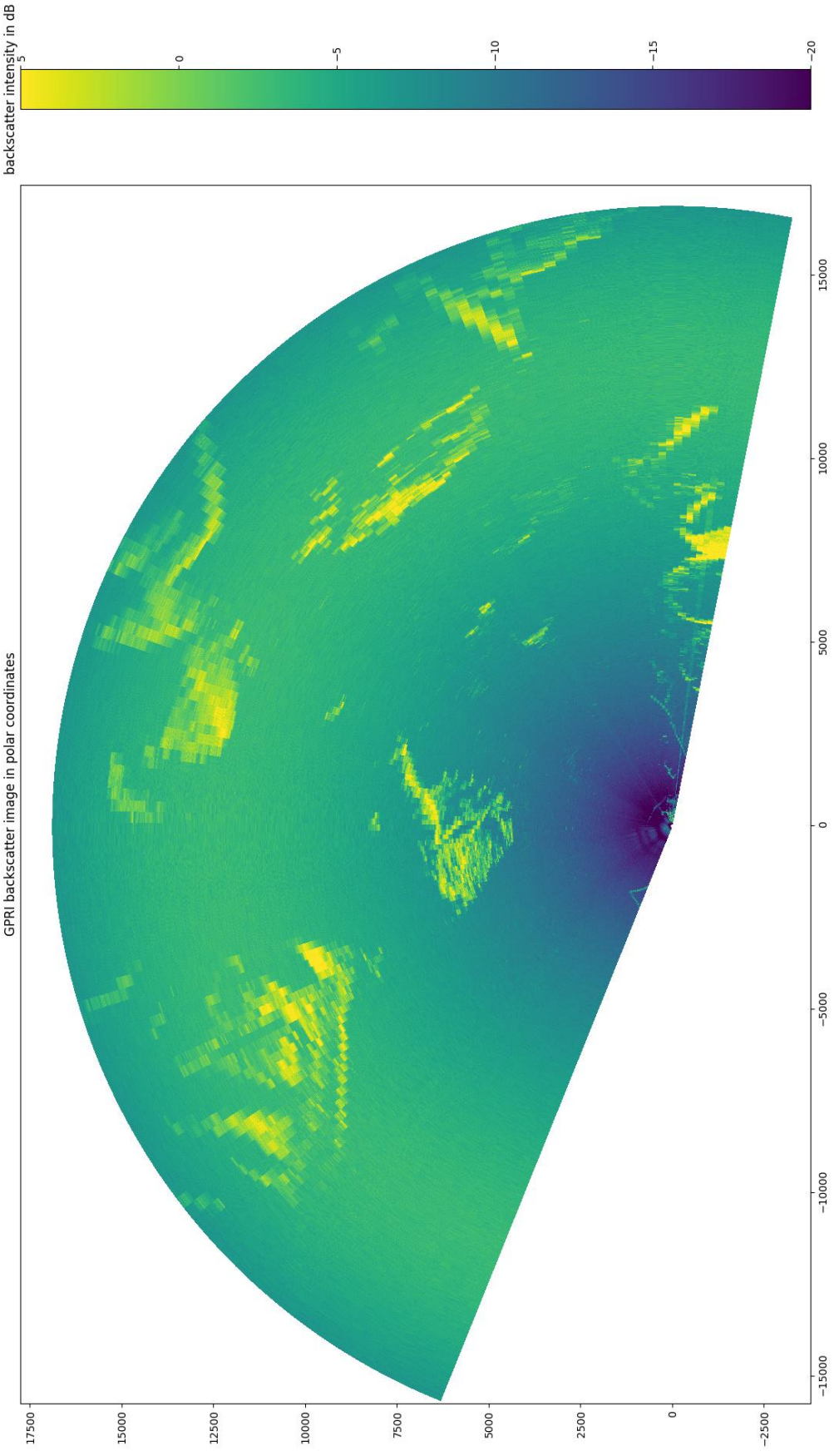

Figure 21: GPRI backscatter image in polar coordinates without processing (from 24.04.2018 15:50:01).

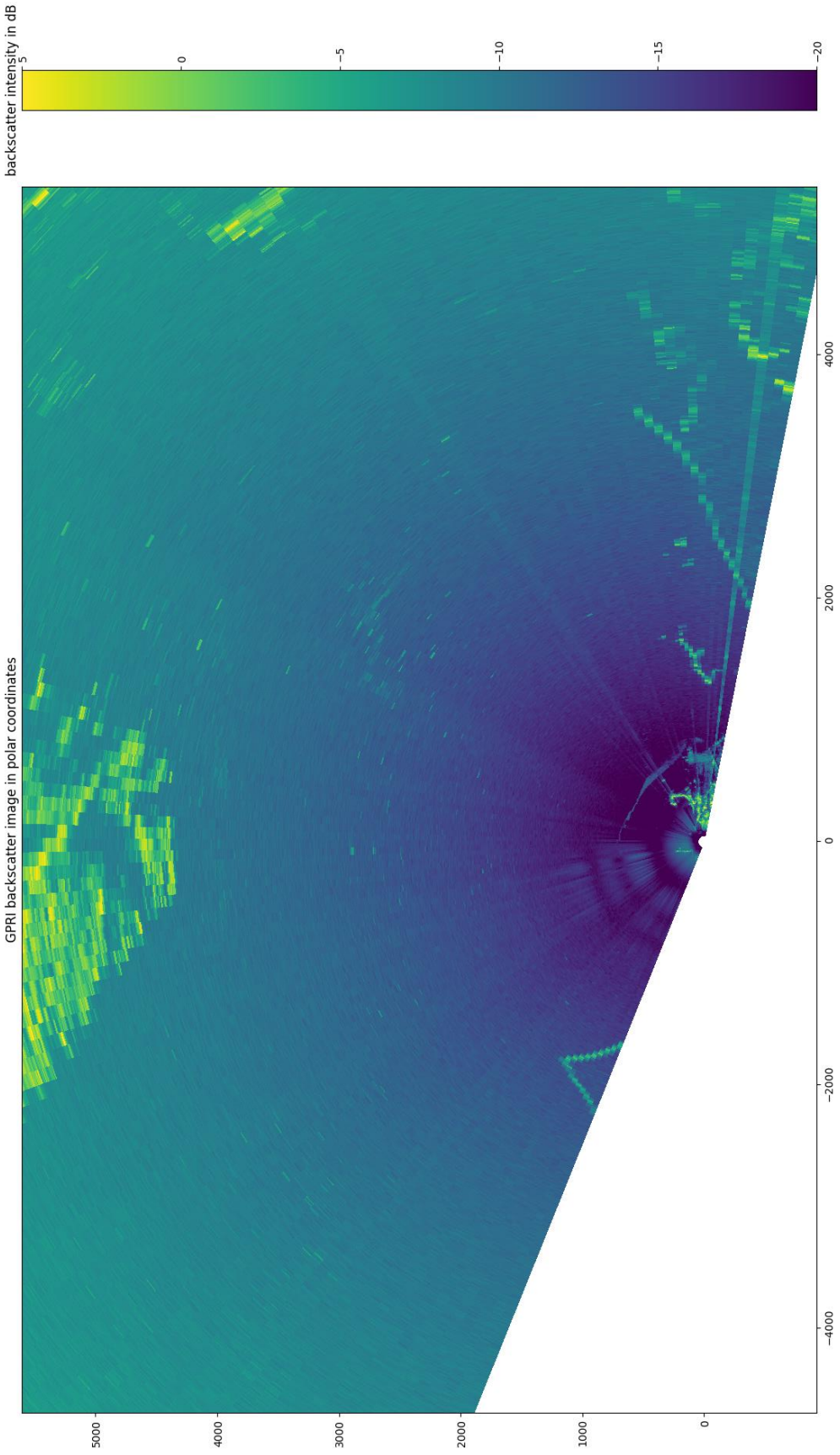

Figure 22: GPRI backscatter image at area of interest in polar coordinates without processing (from 24.04.2018 15:50:01).

In step 2, we remove the variation in backscatter intensity in range direction in the GPRI backscatter image. We average the backscatter intensity for azimuth lines 10 to 60 to form one line in range for all GPRI backscatter images with a temporal resolution of 5 min (figure 23). In detail, we store range times and the corresponding backscatter correction value for those range times in a .npz file. With the compressed array format of the .npz file, we apply the range correction to all GPRI backscatter images.

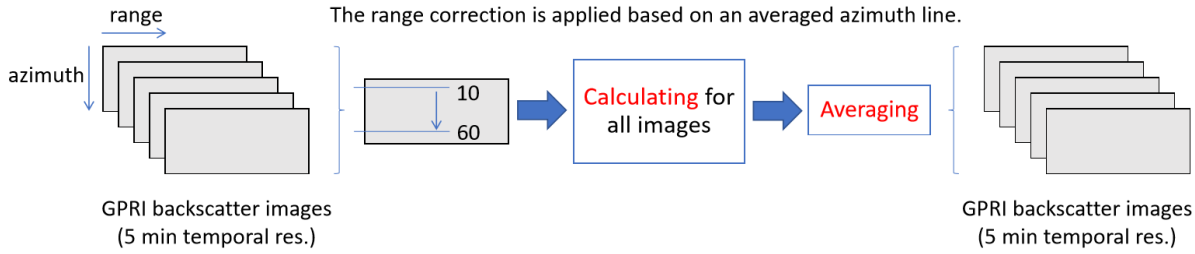

Figure 23: Detrending processing overview.

After the correction of the varying backscatter intensity for all GPRI backscatter images, we can see that the previous backscatter noise floor is diminished (figure 24). Figure 25 is focusing on the area of interest in the corrected GPRI backscatter image. Now, potential iceberg targets and the lagoons in Kongsfjorden are better visible with the even background. From here, it is much more meaningful to work with a threshold dedicated to separate potential iceberg targets from the sea. Both, figure 26 and 27, show the corrected GPRI backscatter image in polar coordinate projections.

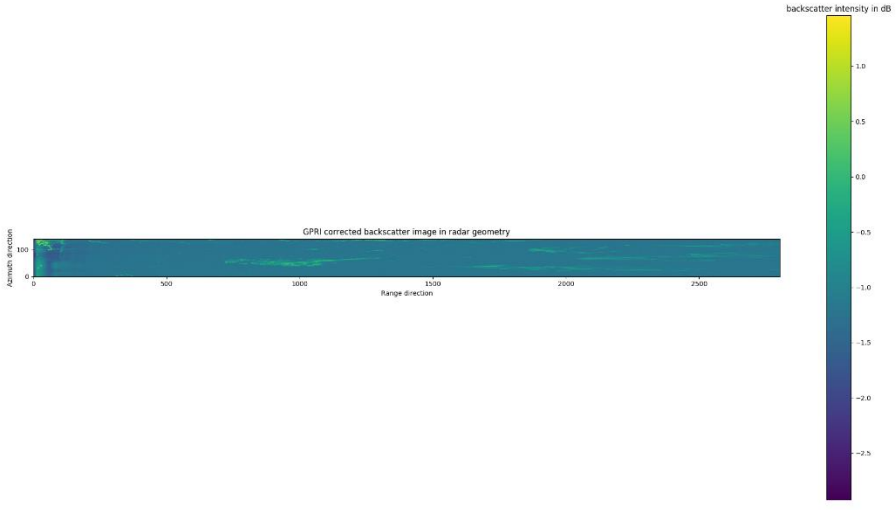

Figure 24: GPRI backscatter image corrected in range direction in radar geometry (from 24.04.2018 15:50:01).

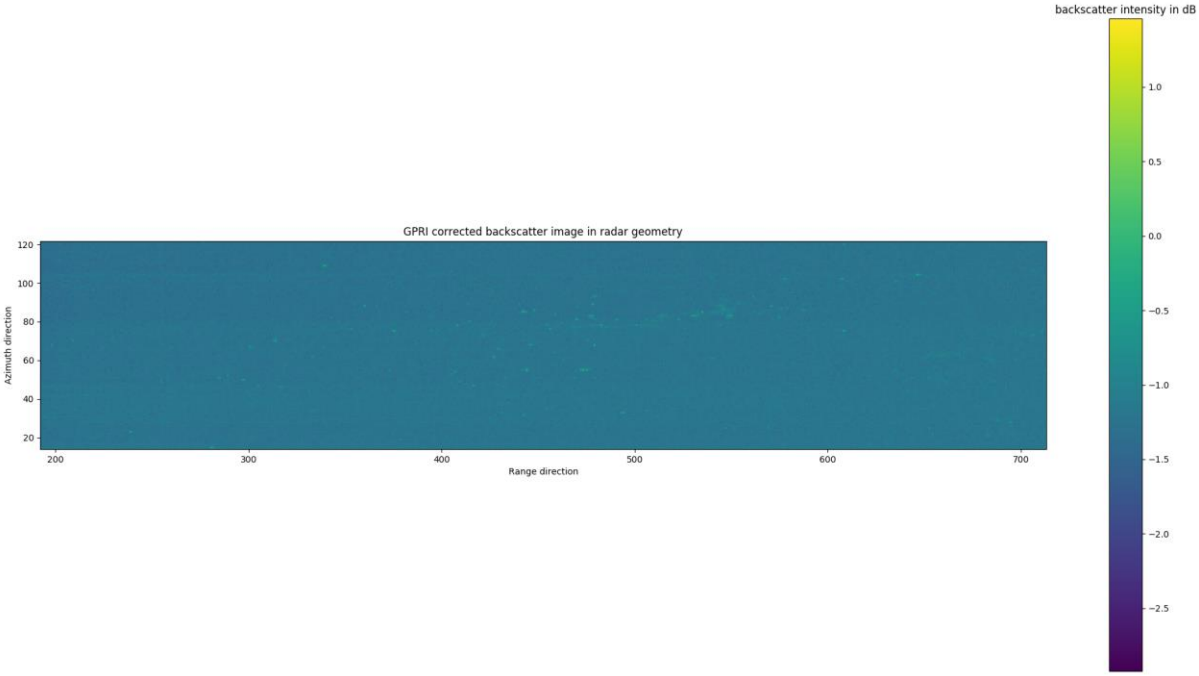

Figure 25: GPRI backscatter image corrected in range direction at area of interest in radar geometry (from 24.04.2018 15:50:01).

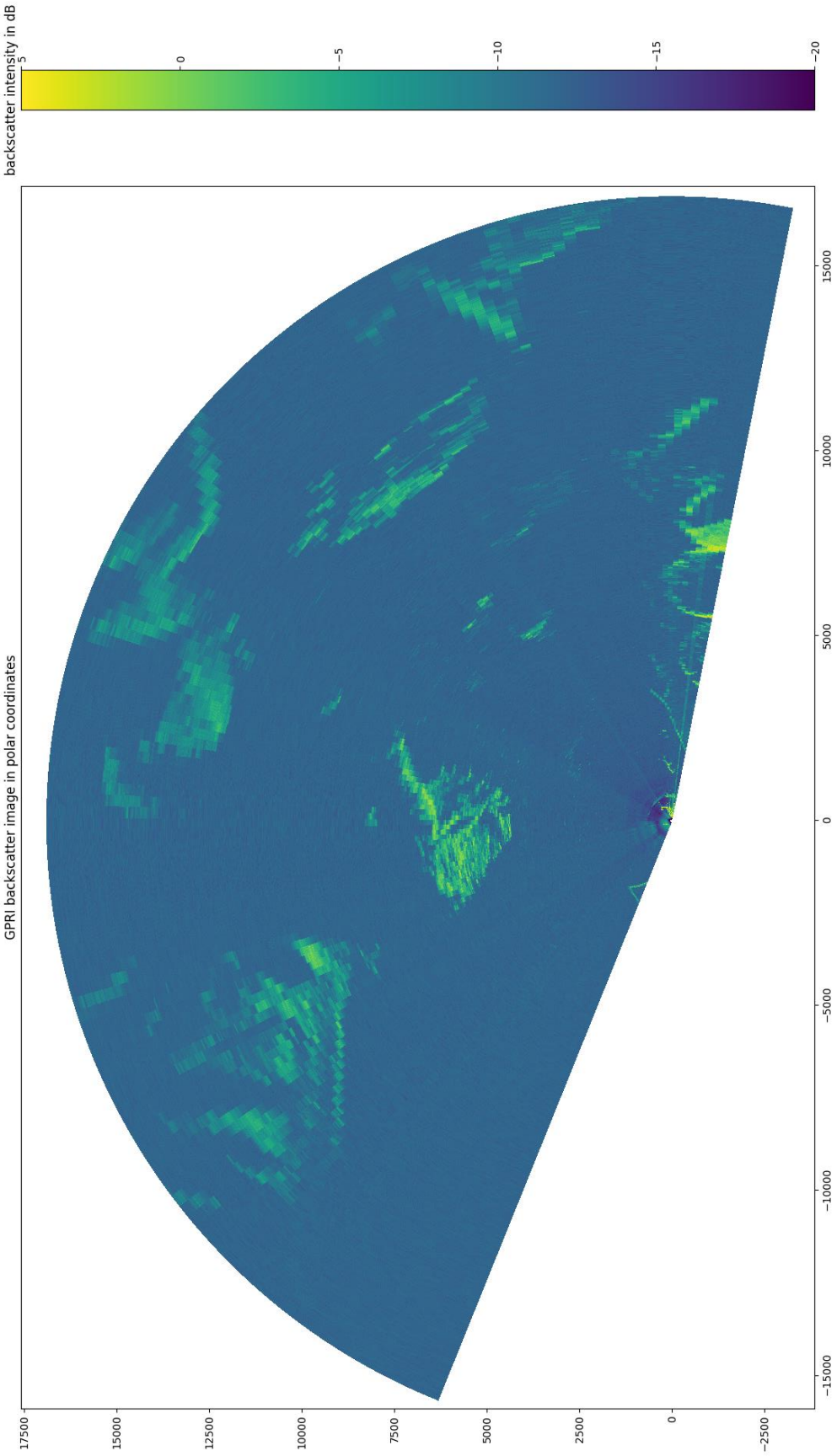

Figure 26: GPRI backscatter image corrected in range in polar coordinates (from 24.04.2018 15:50:01).

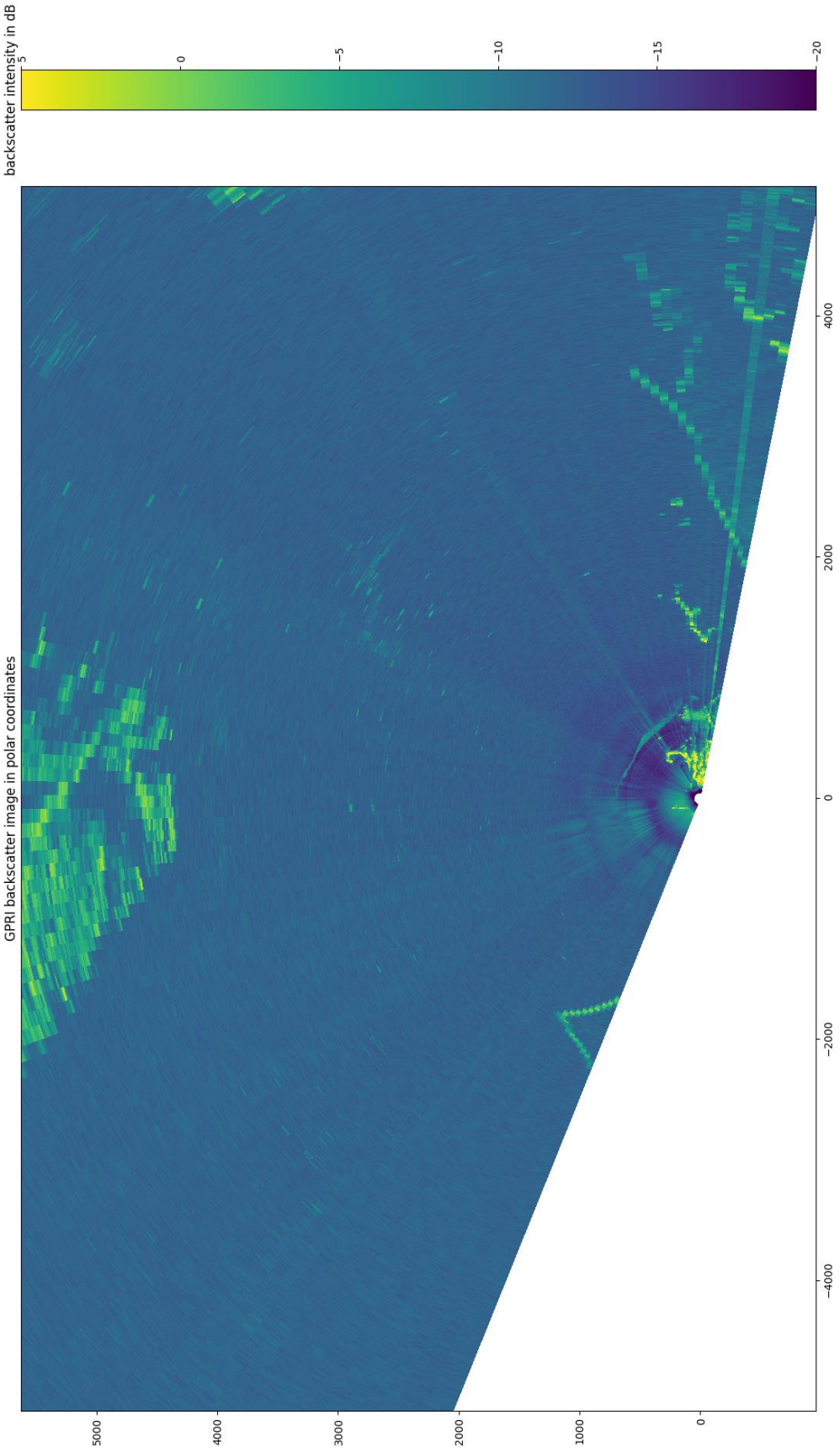

Figure 27: GPRI backscatter image corrected in range at area of interest in polar coordinates (from 24.04.2018 15:50:01).

In step 3 of the main processing chain, we select the area of interest. The GPRI can overlook the entire fjord from its position, but the chosen area of interest is the sea between Ny-Ålesund and Blomstrandhalvøya (figure 28). This accounts for approximately 4.1 km in distance. Solid grounds like for example coastlines and lagoons at both locations will not be taken into account. The focus on only sea surface is beneficial for finding a proper threshold that separates potential iceberg pixels from the background. In addition, the overall processing time is shorter and less processing performance is needed. Our chosen area of interest covers the route that most icebergs and fast-sea-ice are taking to reach the Arctic sea [14]. We can already recognize many potential iceberg targets in the GPRI backscatter image (figure 29).

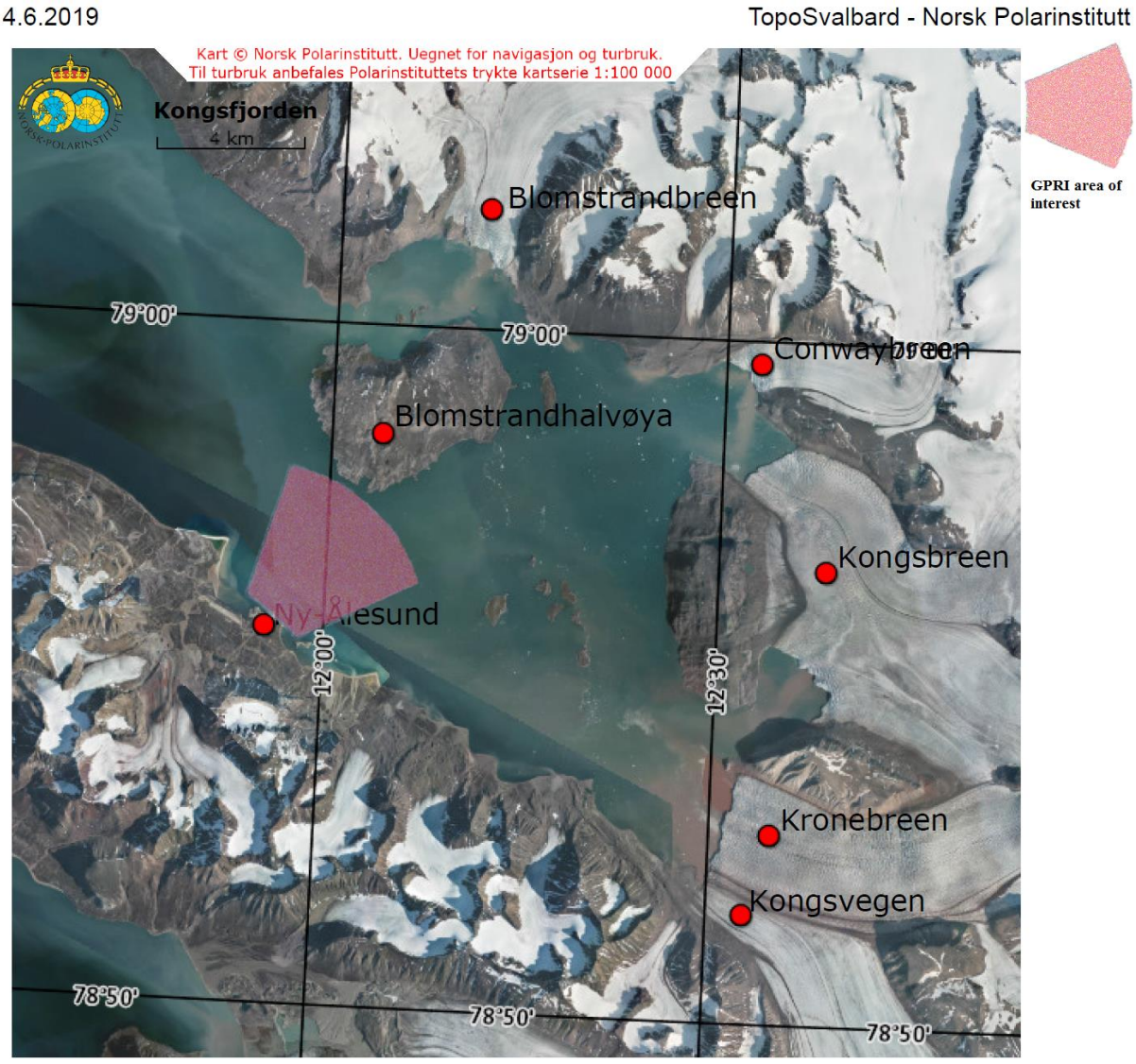

Figure 28: Map of Kongsfjorden in Svalbard including the area of interest (map provided by Norwegian Polar Institute https://toposvalbard.npolar.no/).

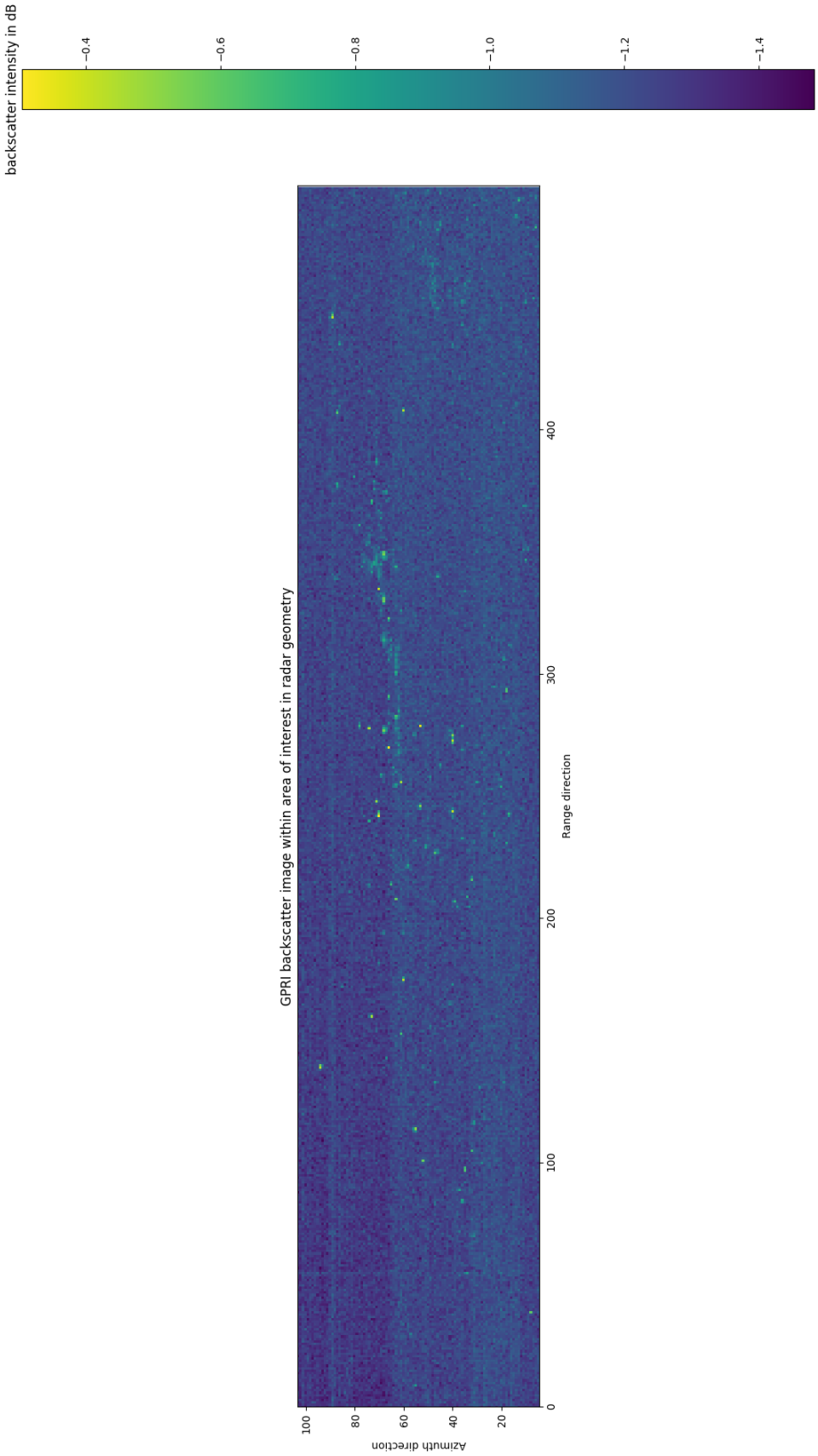

Figure 29: Area of interest within corrected GPRI backscatter image in radar geometry (from 24.04.2018 15:50:01).

Step 4 accounts for the pixel distribution within the chosen area of interest (figure 30). The histogram's pixel distribution has a Gaussian shape with most backscatter intensity values around -1.2. We can clearly say that the majority of pixels belong to the background. As a matter of fact, the histogram shows no clear distinction between potential iceberg pixels and background due to the low iceberg pixel count.

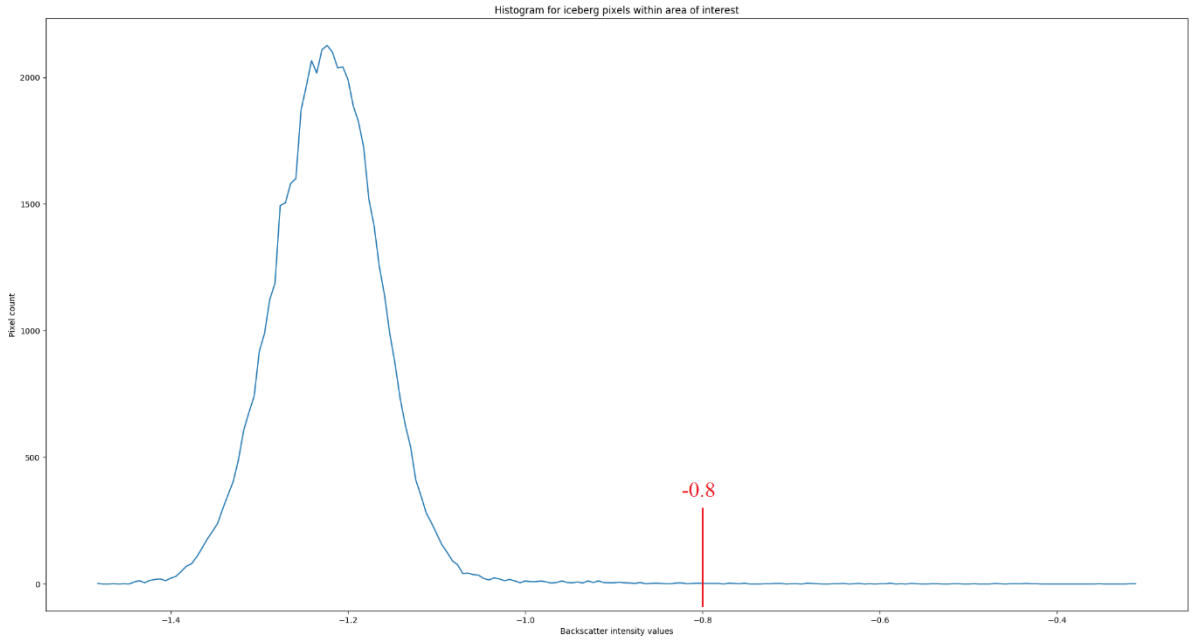

Figure 30: Histogram showing pixel count over backscatter intensity values within the area of interest (from 24.04.2018 15:50:01).

In step 5, we test different thresholds that separate the suspected iceberg targets from the sea in our GPRI backscatter images. There are two methods that can be applied to set the threshold in every GPRI backscatter image: The manual and the automated detection method.

Firstly, we discuss the manual detection method. In the manual detection method, we adjust the threshold for every GPRI backscatter image separately, which means that we are constantly switching between step 5 and 6 of the main processing chain. For example, we have chosen a backscatter intensity value of -0.8 as our final threshold by looking at the GPRI backscatter image (figure 31). From the corresponding histogram, showing only icebergs, we can see that our chosen threshold is almost optimal (figure 32). The optimal threshold is slightly lower at -0.825. In figure 33, we see the histogram for all sea pixels in the GPRI backscatter image separated from the suspected iceberg pixels. As we can see, the manual detection method is subjective and it can take up to several iterative adjustments to find the most optimal threshold.

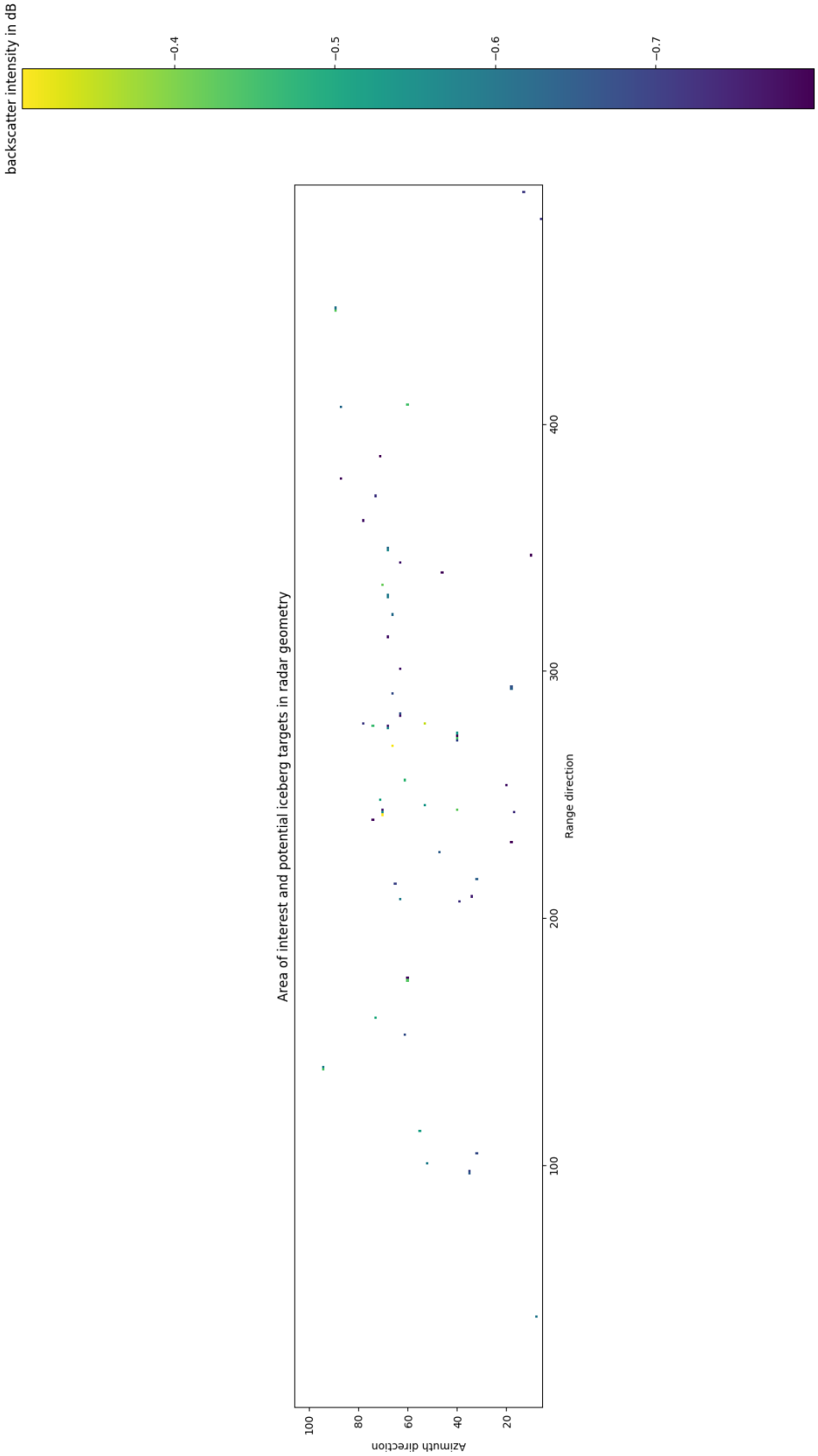

Figure 31: Area of interest within corrected GPRI backscatter image in radar geometry with only detected icebergs after applying the manual detection method (from 24.04.2018 15:50:01).

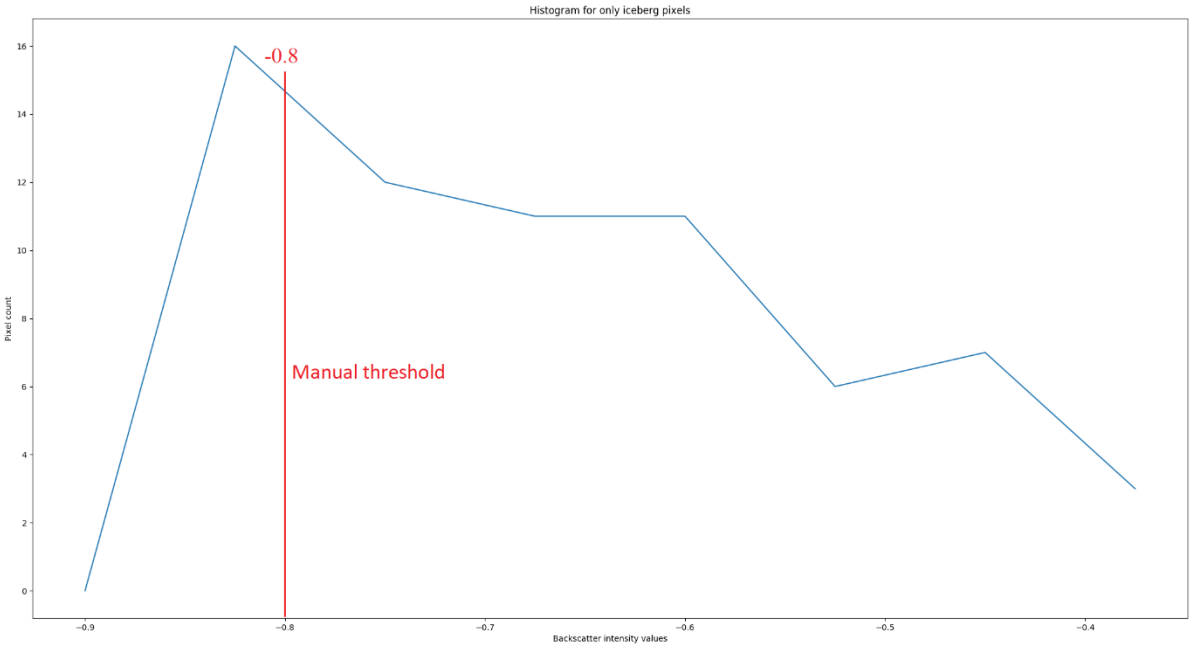

Figure 32: Histogram showing iceberg pixel count over backscatter intensity values within the area of interest (from 24.04.2018 15:50:01).

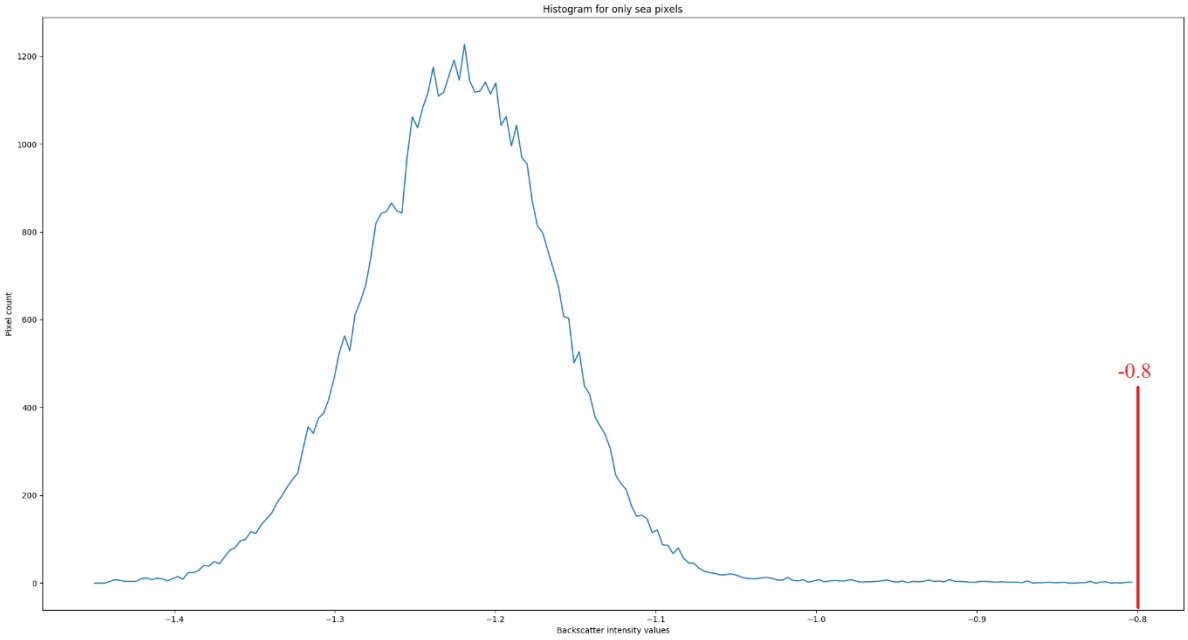

Figure 33: Histogram showing background pixel count over backscatter intensity values within the area of interest (from 24.04.2018 15:50:01).

The automated detection method is used for a large stack of GPRI backscatter images, because we can set the threshold to a certain value to account for the whole GPRI dataset. The automated detection method is the result of experience working with different kind of GPRI backscatter images. For example, GPRI backscatter images might have strong noisy interference due to swell, or the GPRI backscatter images receives clear and strong backscatter

intensities from potential iceberg targets. Either way, the automated detection method accounts for all situations. In general, since most of the potential iceberg pixels have high backscatter intensity values in comparison to the sea background, we can predict that the 99.88th percentile contains most of the iceberg pixels. On the one hand, the 99.88th percentile accounts for the highest backscatter intensity values in the image which leaves us with the big icebergs. On the other hand, it accounts for noisy images that might occur by leaving out most noise. However, it will not include all possible icebergs in the image. For our example GPRI backscatter image from the 24th of April 2018 at 15:50:01, our threshold value at the 99.88th percentile is -0.7927. The backscatter intensity value for the threshold is almost equal to our manually set backscatter intensity value of -0.8. However, from the empirical point of view, the threshold at the 99.88th percentile does not account for GPRI backscatter images with strong interferences.

For step 6 in the main processing chain, we come to the conclusion that we have to increase the threshold to the 99.93th percentile of the backscatter intensity values. This makes sure that less false alarms appear in noisy GPRI backscatter images. Figure 34 shows the result of the new threshold and in contrast to the manual detection method, there is a fewer number of potential iceberg targets.

Finally, step 7 involves georeferencing the processed GPRI backscatter images. The georeferenced GPRI backscatter images can be found in the next chapter.

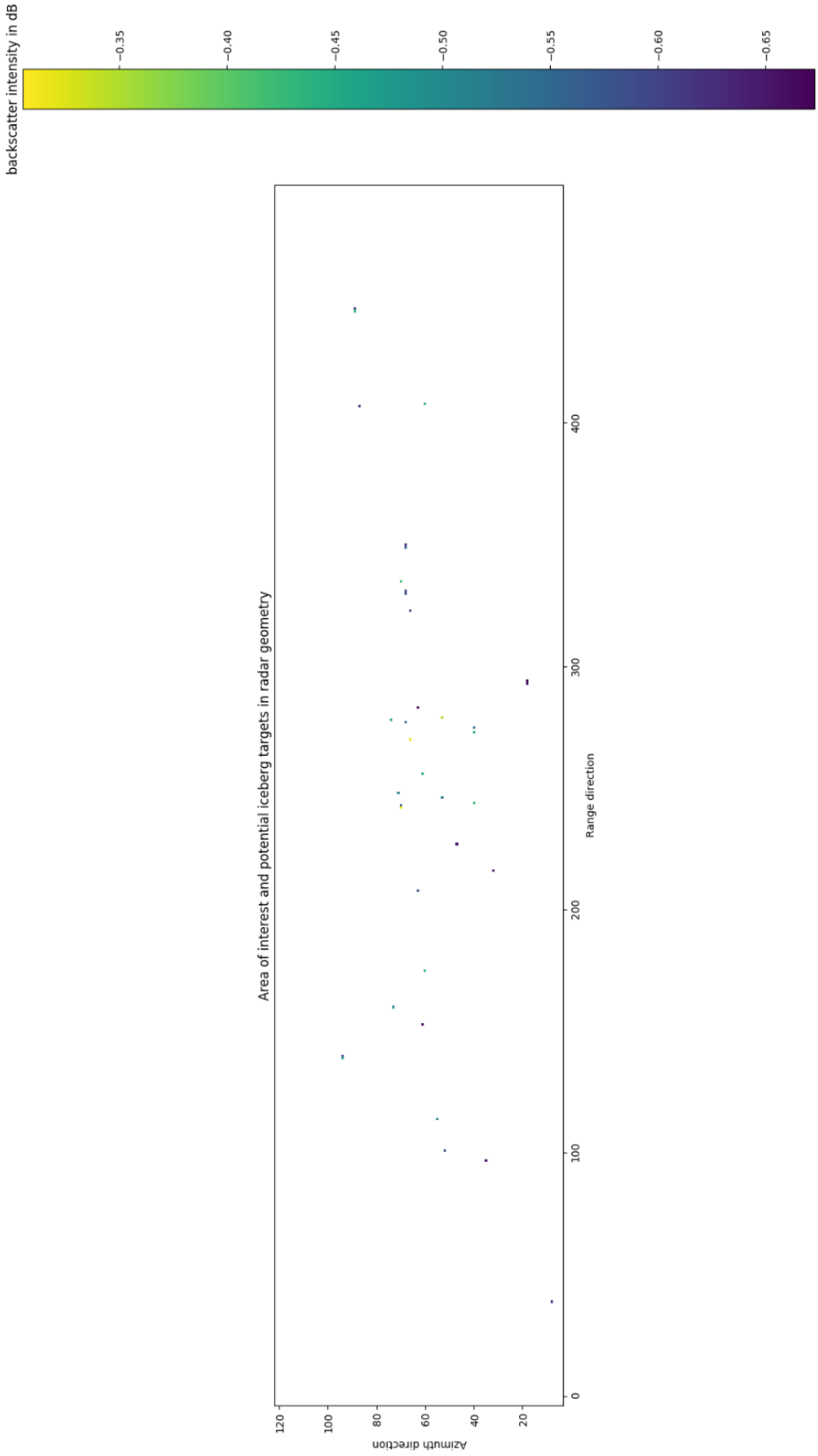

Figure 34: Area of interest within corrected GPRI backscatter image in radar geometry with only detected icebergs after applying the automated detection method (from 24.04.2018 15:50:01).

4 Results

4.1 Results of the detection

After following the 7 steps of the main processing chain, we can analyze the results of the detection methods. Figure 35 shows the georeferenced result of our example GPRI backscatter image from the previous chapter. We added a Sentinel-1 dual-polarized image to the georeferenced result to resemble Kongsfjorden. We zoom in to have a closer look at the detected targets in our area of interest (figure 36). In addition, we can remove the Sentinel-1 image in the background (figure 37). Figure 35 to 37 are showing the results of the manual detection method.

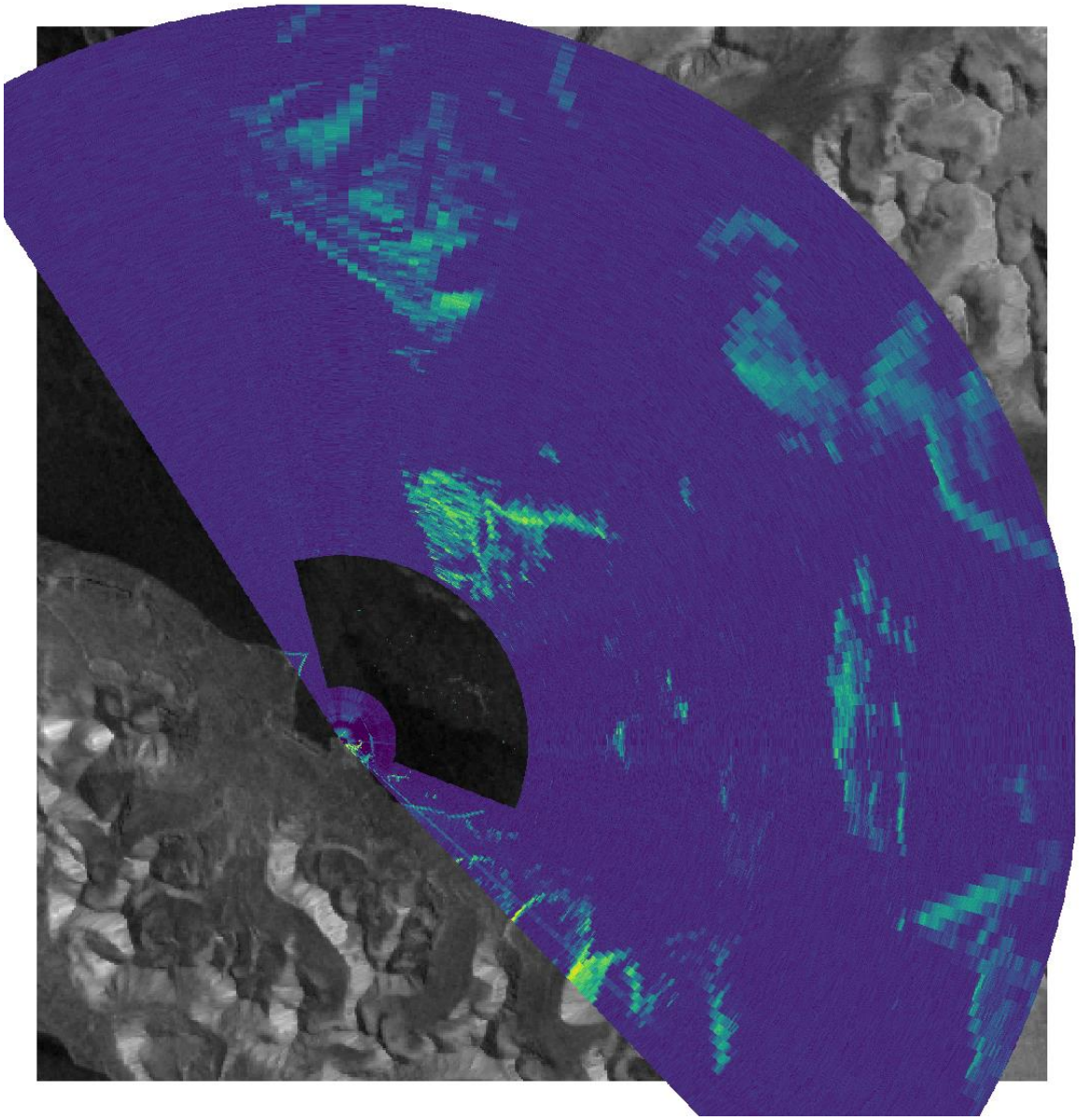

Figure 35: Georeferenced GPRI backscatter intensity image (manual detection method) on top of a Sentinel-1 image (from 24.04.2018 15:50:01).

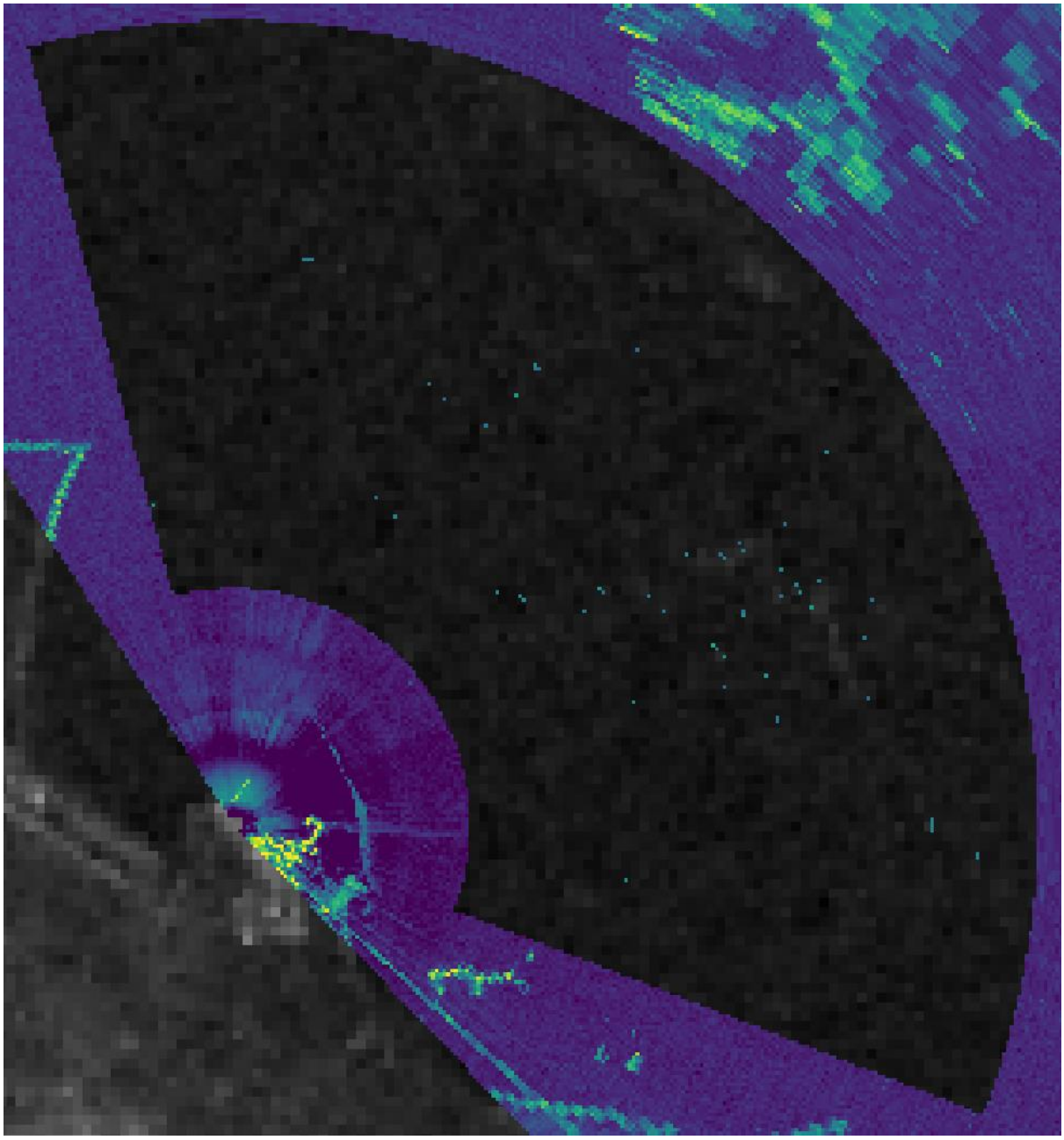

Figure 36: Georeferenced GPRI backscatter intensity image (manual detection method) on top of a Sentinel-1 image at the area of interest (from 24.04.2018 15:50:01).

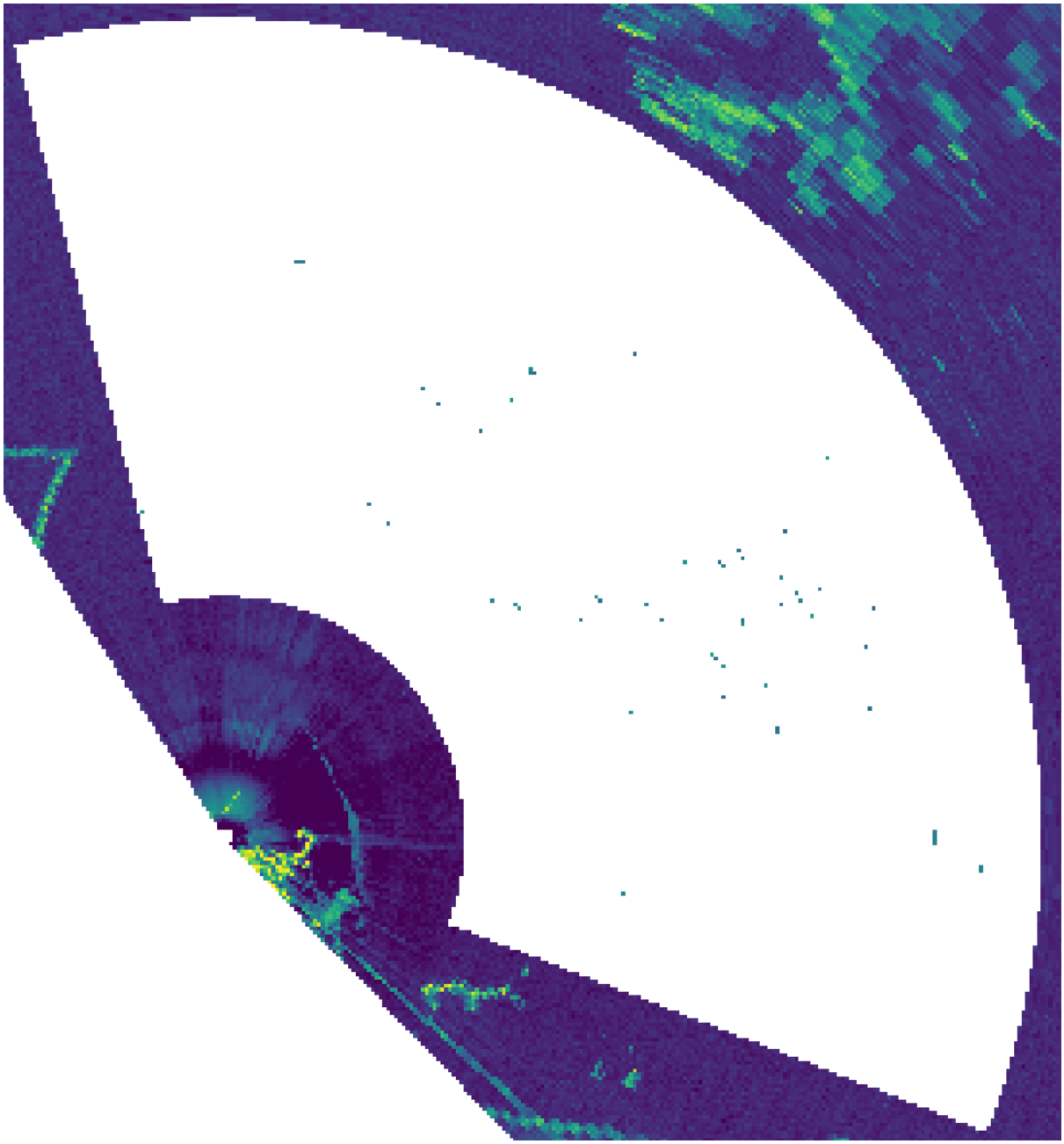

Figure 37: Georeferenced GPRI backscatter intensity image (manual detection method) at the area of interest (from 24.04.2018 15:50:01).

In step 8, after the main processing chain, we can extract all parameters we are interested in. We are focusing on the parameters position, count and size in every processed GPRI backscatter image. The position is related to the GPRI backscatter image radar geometry and not to the georeferenced results. The principle of merging pixels to icebergs is based on direct neighborhood of the pixels (see appendix). First, let us have a look at the extracted parameters from the manual detection method (figure 38). The detection algorithm counted 66 pixels that resemble 44 icebergs in total. On average, most icebergs have the size of 1 or 2 pixels. In contrast, the automated detection method has just 38 pixels that form 33 icebergs (figure 39). The pixel distribution is so sparse that most icebergs have the size of one pixel.

```
...
Pixel count:  66
Iceberg count:  44
Shape of aoi:  (105, 500)
...
Iceberg number:  0 .. Size:  1 .. Average position:  (39.0, 8.0)
Iceberg number:  1 .. Size:  1 .. Average position:  (81.0, 0.0)
Iceberg number:  2 .. Size:  1 .. Average position:  (97.0, 35.0)
Iceberg number:  3 .. Size:  1 .. Average position:  (98.0, 35.0)
Iceberg number:  4 .. Size:  7 .. Average position:  (233.28571428571428, 63.57142857142857)
Iceberg number:  5 .. Size:  1 .. Average position:  (105.0, 32.0)
Iceberg number:  6 .. Size:  1 .. Average position:  (114.0, 55.0)
Iceberg number:  7 .. Size:  3 .. Average position:  (206.0, 61.0)
Iceberg number:  8 .. Size:  1 .. Average position:  (140.0, 94.0)
Iceberg number:  9 .. Size:  1 .. Average position:  (160.0, 73.0)
Iceberg number:  10 .. Size:  1 .. Average position:  (175.0, 60.0)
Iceberg number:  11 .. Size:  1 .. Average position:  (176.0, 60.0)
Iceberg number:  12 .. Size:  4 .. Average position:  (235.25, 50.5)
Iceberg number:  13 .. Size:  1 .. Average position:  (208.0, 63.0)
Iceberg number:  14 .. Size:  10 .. Average position:  (302.4, 52.5)
Iceberg number:  15 .. Size:  2 .. Average position:  (232.0, 51.5)
Iceberg number:  16 .. Size:  3 .. Average position:  (257.6666666666667, 42.333333333333336)
Iceberg number:  17 .. Size:  2 .. Average position:  (277.0, 71.0)
Iceberg number:  18 .. Size:  1 .. Average position:  (242.0, 70.0)
Iceberg number:  19 .. Size:  1 .. Average position:  (254.0, 20.0)
Iceberg number:  20 .. Size:  1 .. Average position:  (256.0, 61.0)
Iceberg number:  21 .. Size:  1 .. Average position:  (270.0, 66.0)
Iceberg number:  22 .. Size:  2 .. Average position:  (293.5, 54.0)
Iceberg number:  23 .. Size:  2 .. Average position:  (294.5, 54.0)
Iceberg number:  24 .. Size:  2 .. Average position:  (311.0, 65.5)
Iceberg number:  25 .. Size:  2 .. Average position:  (314.0, 71.0)
Iceberg number:  26 .. Size:  1 .. Average position:  (283.0, 63.0)
Iceberg number:  27 .. Size:  1 .. Average position:  (291.0, 66.0)
Iceberg number:  28 .. Size:  1 .. Average position:  (293.0, 18.0)
Iceberg number:  29 .. Size:  1 .. Average position:  (294.0, 18.0)
Iceberg number:  30 .. Size:  1 .. Average position:  (301.0, 63.0)
Iceberg number:  31 .. Size:  2 .. Average position:  (355.0, 68.5)
Iceberg number:  32 .. Size:  1 .. Average position:  (331.0, 68.0)
Iceberg number:  33 .. Size:  1 .. Average position:  (335.0, 70.0)
Iceberg number:  34 .. Size:  2 .. Average position:  (363.5, 58.5)
Iceberg number:  35 .. Size:  1 .. Average position:  (347.0, 10.0)
Iceberg number:  36 .. Size:  1 .. Average position:  (349.0, 68.0)
Iceberg number:  37 .. Size:  1 .. Average position:  (361.0, 78.0)
Iceberg number:  38 .. Size:  1 .. Average position:  (371.0, 73.0)
Iceberg number:  39 .. Size:  1 .. Average position:  (378.0, 87.0)
Iceberg number:  40 .. Size:  1 .. Average position:  (408.0, 60.0)
Iceberg number:  41 .. Size:  1 .. Average position:  (446.0, 89.0)
Iceberg number:  42 .. Size:  1 .. Average position:  (447.0, 89.0)
Iceberg number:  43 .. Size:  1 .. Average position:  (483.0, 6.0)
```

Figure 38: Iceberg parameters from the area of interest of the manually processed GPRI backscatter image (from 24.04.2018 15:50:01).

```
...
Pixel count:  38
Iceberg count:  33
Shape of aoi:  (105, 500)
...
Iceberg number:  0 .. Size:  1 .. Average position:  (39.0, 8.0)
Iceberg number:  1 .. Size:  1 .. Average position:  (81.0, 0.0)
Iceberg number:  2 .. Size:  1 .. Average position:  (97.0, 35.0)
Iceberg number:  3 .. Size:  2 .. Average position:  (127.0, 56.5)
Iceberg number:  4 .. Size:  1 .. Average position:  (114.0, 55.0)
Iceberg number:  5 .. Size:  1 .. Average position:  (139.0, 94.0)
Iceberg number:  6 .. Size:  1 .. Average position:  (140.0, 94.0)
Iceberg number:  7 .. Size:  1 .. Average position:  (160.0, 73.0)
Iceberg number:  8 .. Size:  1 .. Average position:  (175.0, 60.0)
Iceberg number:  9 .. Size:  1 .. Average position:  (208.0, 63.0)
Iceberg number:  10 .. Size:  3 .. Average position:  (236.66666666666666, 52.0)
Iceberg number:  11 .. Size:  1 .. Average position:  (227.0, 47.0)
Iceberg number:  12 .. Size:  1 .. Average position:  (242.0, 70.0)
Iceberg number:  13 .. Size:  1 .. Average position:  (243.0, 70.0)
Iceberg number:  14 .. Size:  1 .. Average position:  (244.0, 40.0)
Iceberg number:  15 .. Size:  1 .. Average position:  (256.0, 61.0)
Iceberg number:  16 .. Size:  1 .. Average position:  (270.0, 66.0)
Iceberg number:  17 .. Size:  1 .. Average position:  (273.0, 40.0)
Iceberg number:  18 .. Size:  1 .. Average position:  (275.0, 40.0)
Iceberg number:  19 .. Size:  1 .. Average position:  (277.0, 68.0)
Iceberg number:  20 .. Size:  2 .. Average position:  (314.0, 71.0)
Iceberg number:  21 .. Size:  2 .. Average position:  (304.5, 60.5)
Iceberg number:  22 .. Size:  1 .. Average position:  (283.0, 63.0)
Iceberg number:  23 .. Size:  1 .. Average position:  (293.0, 18.0)
Iceberg number:  24 .. Size:  1 .. Average position:  (294.0, 18.0)
Iceberg number:  25 .. Size:  1 .. Average position:  (323.0, 66.0)
Iceberg number:  26 .. Size:  1 .. Average position:  (331.0, 68.0)
Iceberg number:  27 .. Size:  1 .. Average position:  (335.0, 70.0)
Iceberg number:  28 .. Size:  1 .. Average position:  (349.0, 68.0)
Iceberg number:  29 .. Size:  1 .. Average position:  (407.0, 87.0)
Iceberg number:  30 .. Size:  1 .. Average position:  (408.0, 60.0)
Iceberg number:  31 .. Size:  1 .. Average position:  (446.0, 89.0)
Iceberg number:  32 .. Size:  1 .. Average position:  (447.0, 89.0)
```

Figure 39: Iceberg parameters from the area of interest of the automated processed GPRI backscatter image (from 24.04.2018 15:50:01).

4.2 Validation with Auxiliary Data

We present our findings in three example validations.

The first example is the georeferenced GPRI backscatter image taken on the 19th of April 2018 at 15:30:01. The auxiliary data which is used for validation is coming from a Radarsat-2 image. The satellite SAR sensor of Radarsat-2 acquired its image 37 seconds after the GPRI did. The overall result is presented in figure 40. If we zoom further into the scene, we can see detected iceberg within the area of interest (figure 41). The current GPRI backscatter image was processed with the manual detection method. In order to make a better comparison between manual and automated detection method, we take a smaller investigation area (orange box). Both, automated and manual detection method are presented in figures 42 and 43 respectively. In order to distinguish from the Radarsat-2 image in the background, the color of the detected icebergs was changed to light blue.

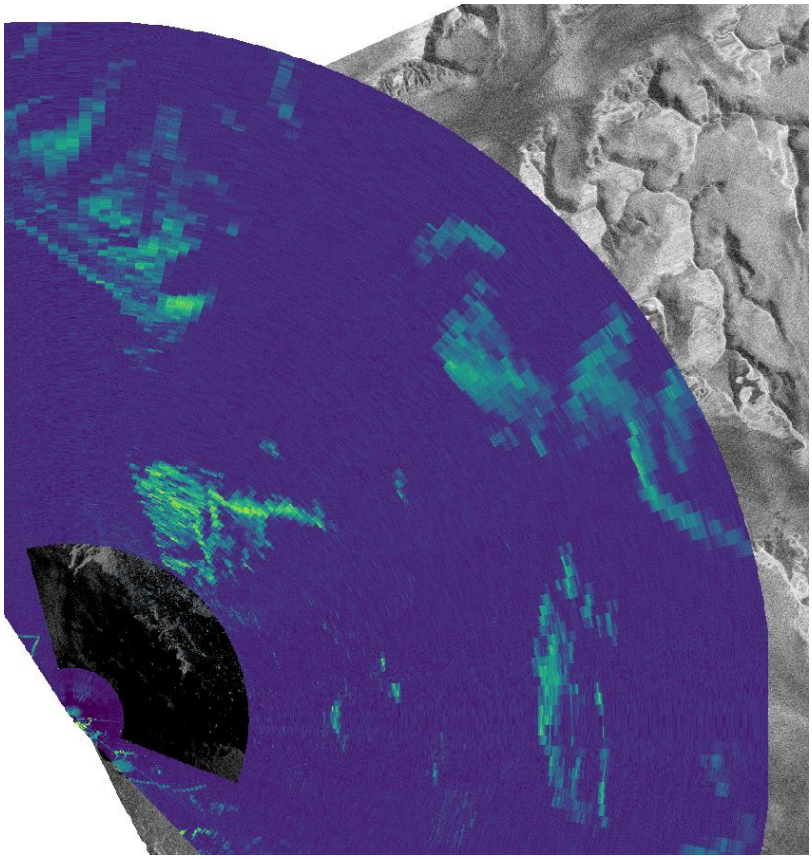

Figure 40: Processed GPRI backscatter image and Radarsat-2 image in the background (from 19.04.2018 15:30:01).

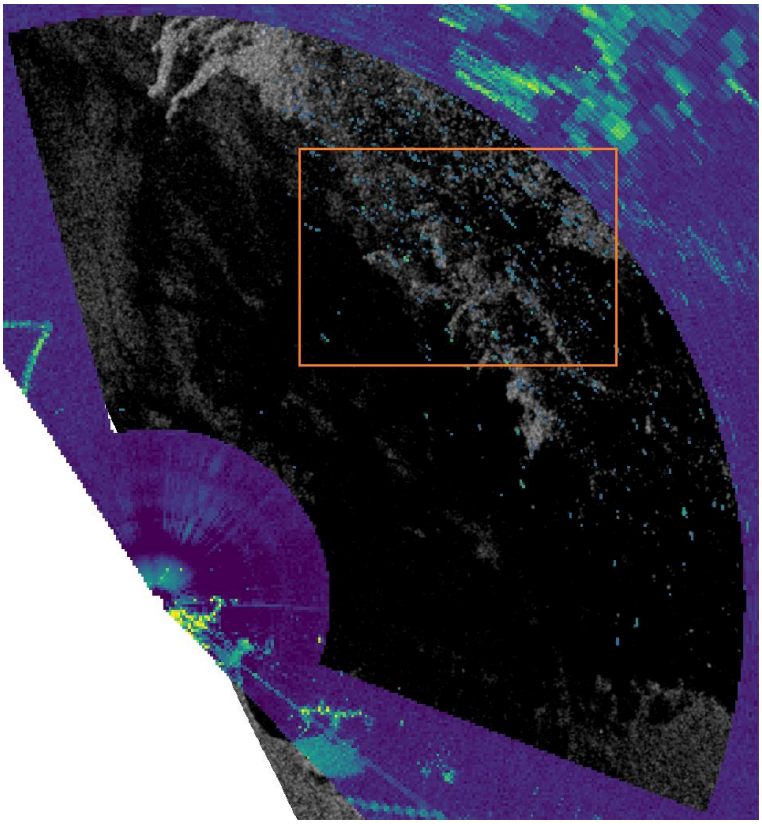

Figure 41: Focus on area of interest of the processed GPRI backscatter image (from 19.04.2018 15:30:01).

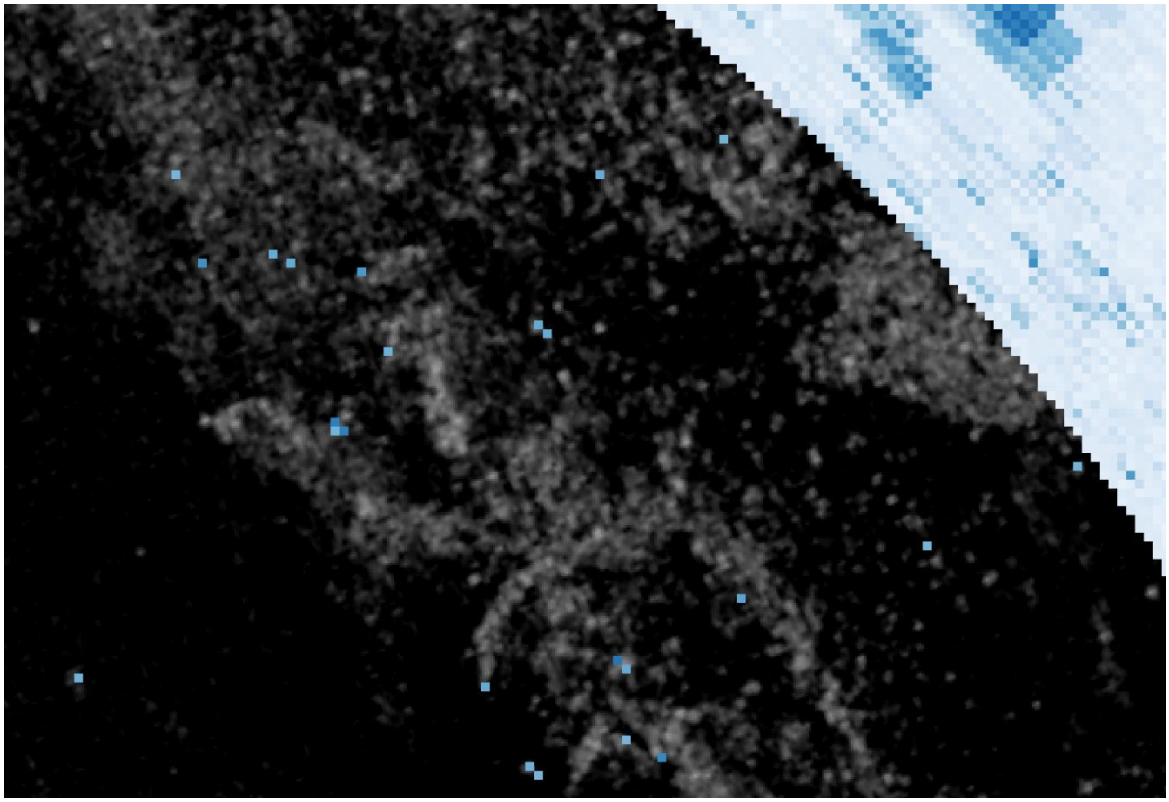

Figure 42: Automated detection method (from 19.04.2018 15:30:01).

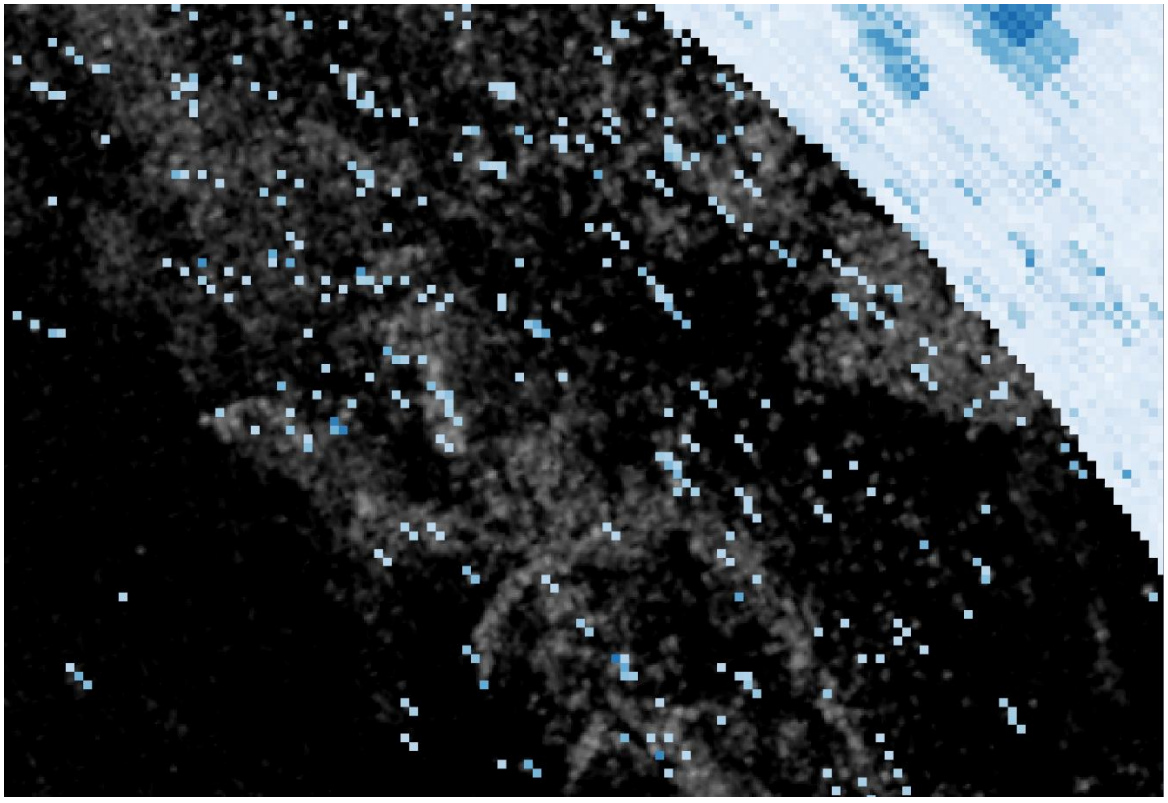

Figure 43: Manual detection method (from 19.04.2018 15:30:01).

We can observe that the manual detection method has more potential iceberg targets in the georeferenced GPRI backscatter image than for the automated detection method. The most important iceberg parameters are presented in table 3. The result of the manual detection method is more reasonable by comparing it with the Radarsat-2 image taken at 15:30:38.

Table 3: Iceberg parameter comparison (from 19.04.2018 15:30:01).

Parameters	Automated detection	Manual detection
Pixel count	38	479
Iceberg count	33	74
Largest iceberg size	3 pixels	176 pixels

In figure 44, we polygonise our raster data to vector data, which makes it possible to compare both detection methods with the auxiliary data from Radarsat-2. The numerous yellow polygons are potential iceberg targets detected with the manual detection method. In contrast, the results from the automated detection are represented as blue polygons. We can calculate the centroid data from the vectorized dataset (figure 45).

In general, the Radarsat-2 image shows more detected icebergs than the georeferenced GPRI backscatter image which was processed with the manual detection method. Some of the detected icebergs in the georeferenced GPRI backscatter image are slightly shifted in position from the icebergs detected by Radarsat-2. These minor position changes are probably caused by the time delay of 37 seconds between both acquisitions.

The Radarsat-2 image shows more potential iceberg targets than the georeferenced GPRI backscatter image. That is because the GPRI antenna has a worse spatial resolution in azimuth. At more than 3 km distance, the GPRI has an azimuth resolution of 21 m. In comparison, Radarsat-2 acquired the validation image with a spatial resolution of 11x9 m, which makes it easier to detect more potential icebergs.

We cannot be certain from the georeferenced GPRI backscatter image that we did not detect false positive pixels, but the majority of the manually detected iceberg pixels were validated by the Radarsat-2 image (figure 44).

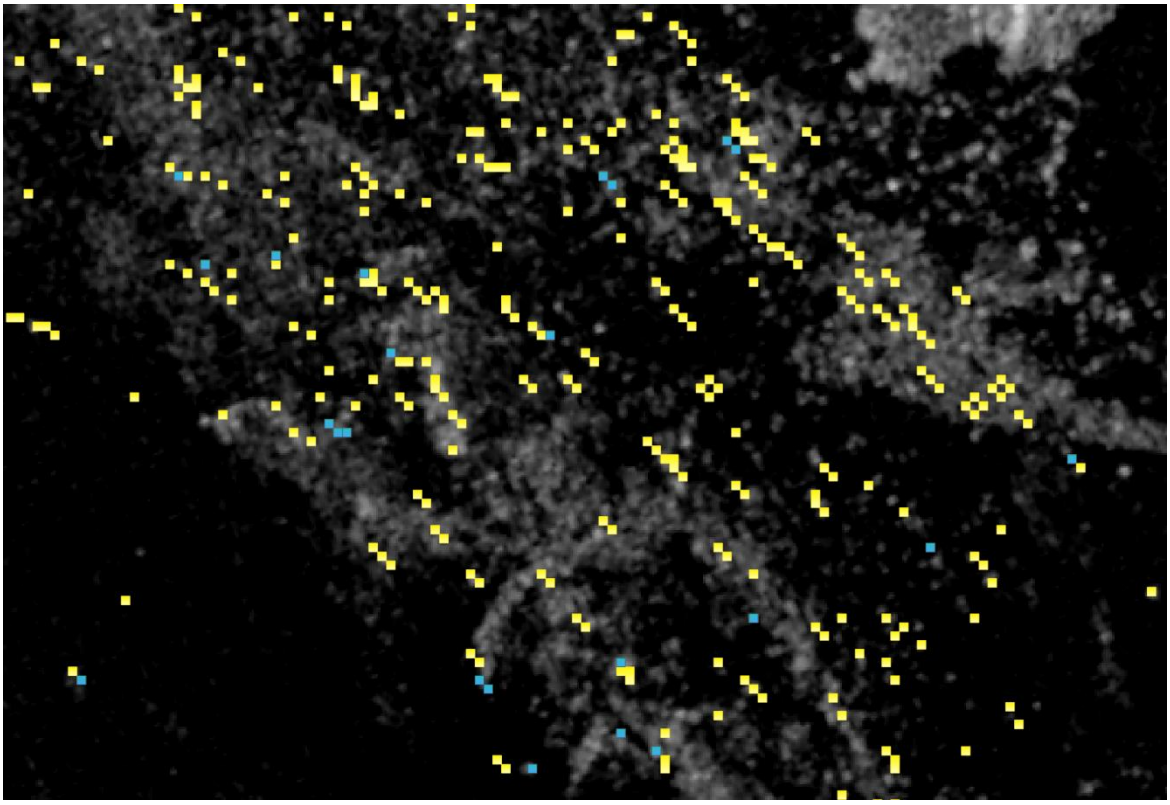

Figure 44: Comparison of both detection methods with vectorized data (from 19.04.2018 15:30:01).

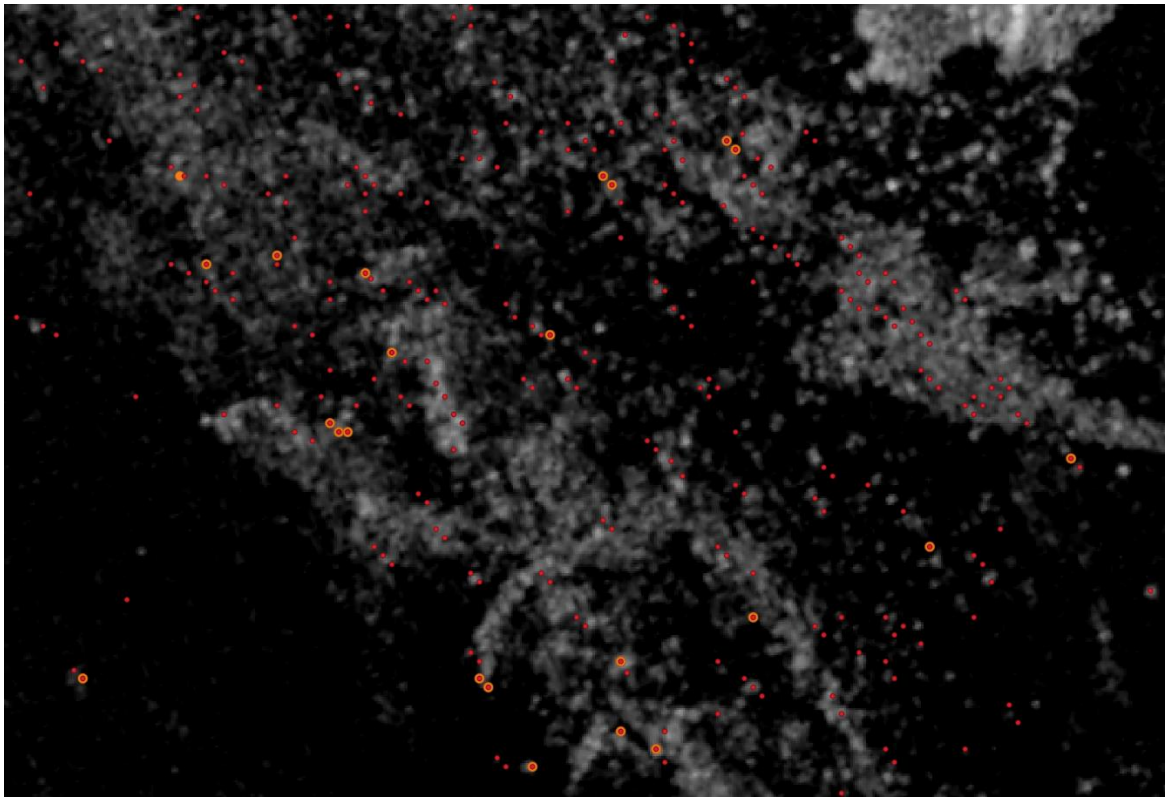

Figure 45: Centroid positions of manual (red dots) and automated (orange dots) detection method (from 19.04.2018 15:30:01).

In the second validation example, we have a look at the UAV imagery. The RGB camera FLIR PtGrey Chameleon 2 has acquired an image on the 24th of April 2018 at 15:50 (figure 46). The position of the UAV at that time was at Latitude 78.937395 deg and Longitude 12.035352 deg. The georeferenced GPRI image was taken from the same day at 15:50:01 and the manual detection method was applied to it beforehand (figure 47). The Sentinel-1A image in the background is an IWS product which was acquired on the 24th of April at 15:45:35. The Sentinel-1A resolution is too poor for a validation, but the UAV coordinates where of use to validate the position of the four detected pixels in figure 48.

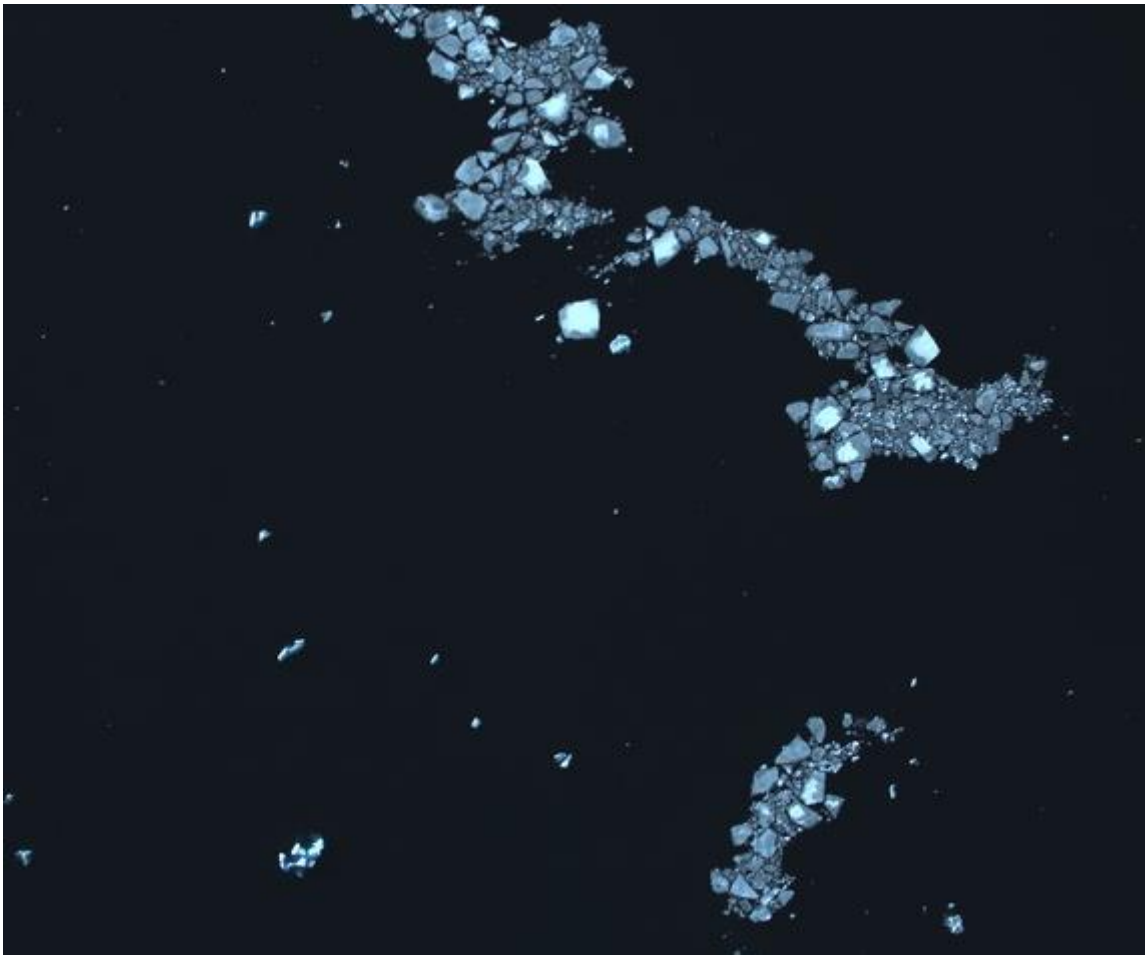

Figure 46: Icebergs detected by the FLIR PtGrey Chameleon 2 mounted on the UAV (from 24.04.2018 15:50).

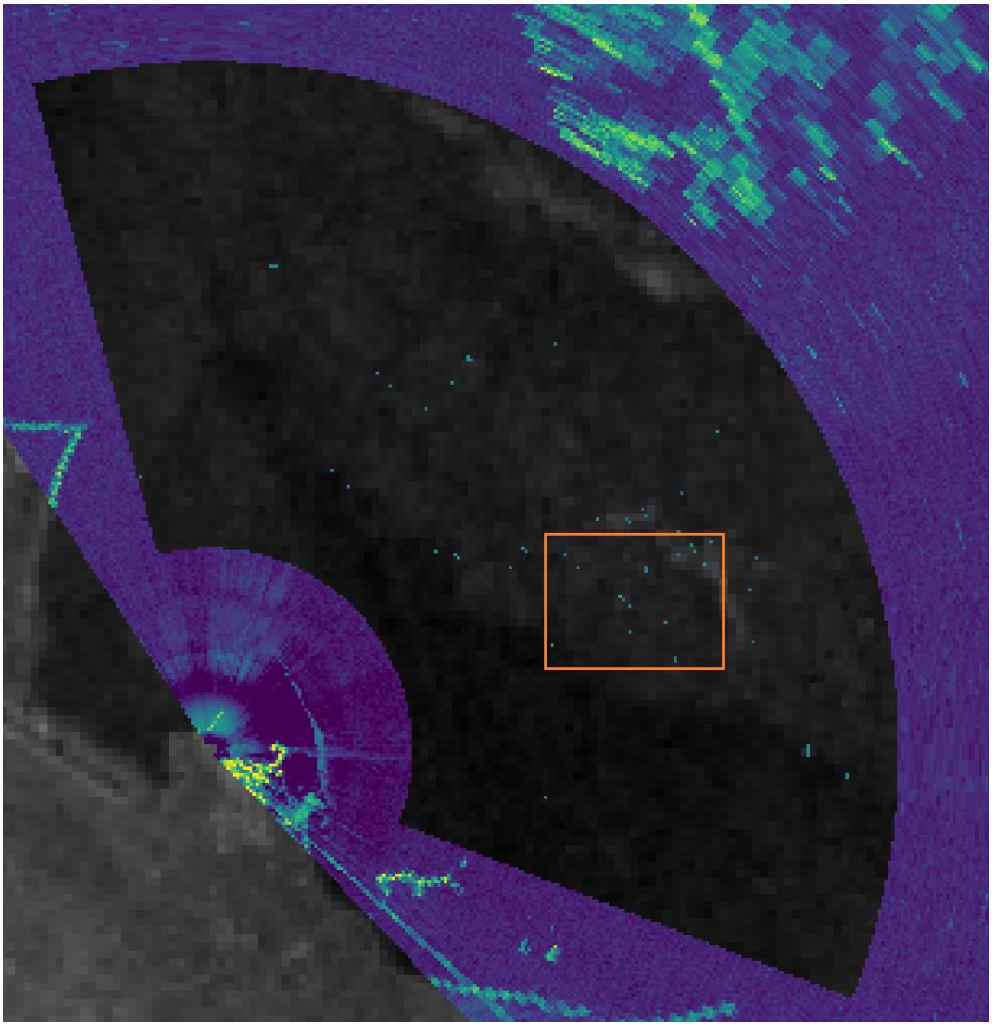

Figure 47: Georeferenced GPRI backscatter image (manual detection method) and Sentinel-1A image (HH polarization) in the background (from 24.04.2018 15:50:01).

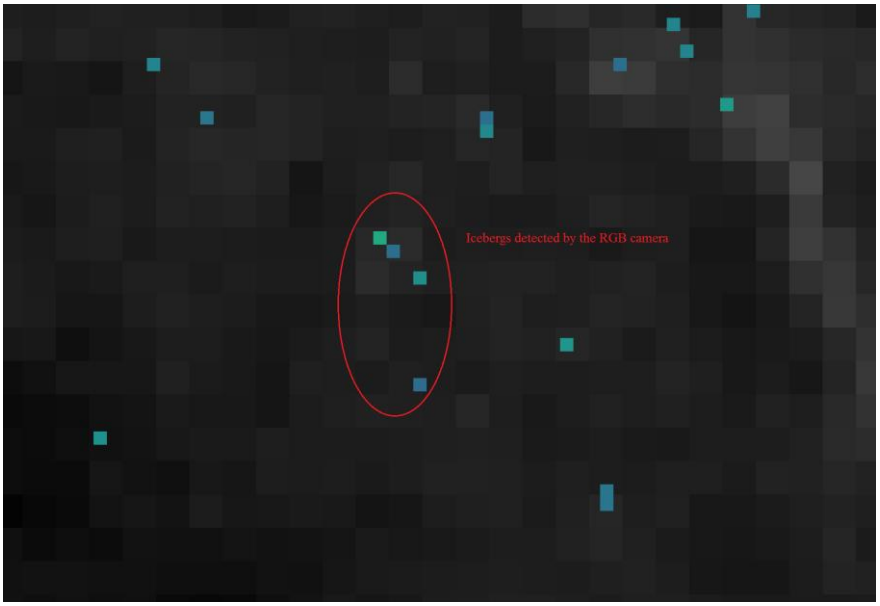

Figure 48: Focus on the location where the UAV has been at the same time (from 24.04.2018 15:50:01).

The third example takes the NPI boat tracks into account. We know that NPI circumnavigated two icebergs within our area of interest on the 19th of April 2018 at 12:12:00 UTC (iceberg 1) and at 12:14:00 UTC (iceberg 2) (figure 49 and 50). The circumnavigated icebergs were detected by the georeferenced GPRI backscatter image (figure 51). The GPRI backscatter image was taken on the same day at 12:15:01 and the manual detection method was applied to it. Although the iceberg pixel positions are slightly shifted in the georeferenced GPRI image, we can assume that iceberg 1 and iceberg 2 were the icebergs that NPI circumnavigated (figure 52).

Figure 49: First circumnavigated iceberg 1 (from 19.04.2018 12:12:00).

Figure 50: Second circumnavigated iceberg 2 (from 19.04.2018 12:14:00).

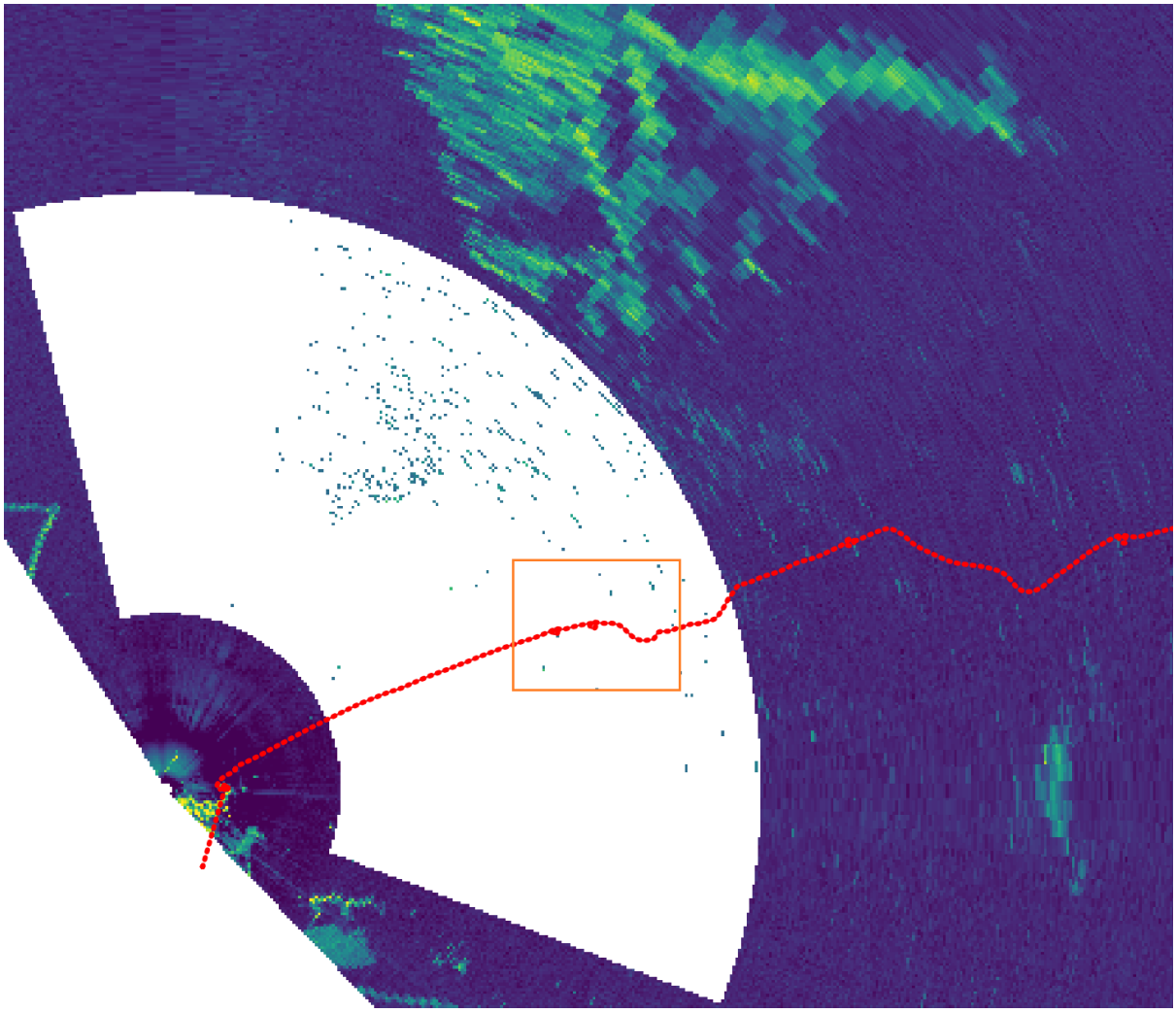

Figure 51: NPI boat track (red dotted line) with georeferenced GPRI backscatter image (manual detection method) (from 19.04.2018 12:15:01).

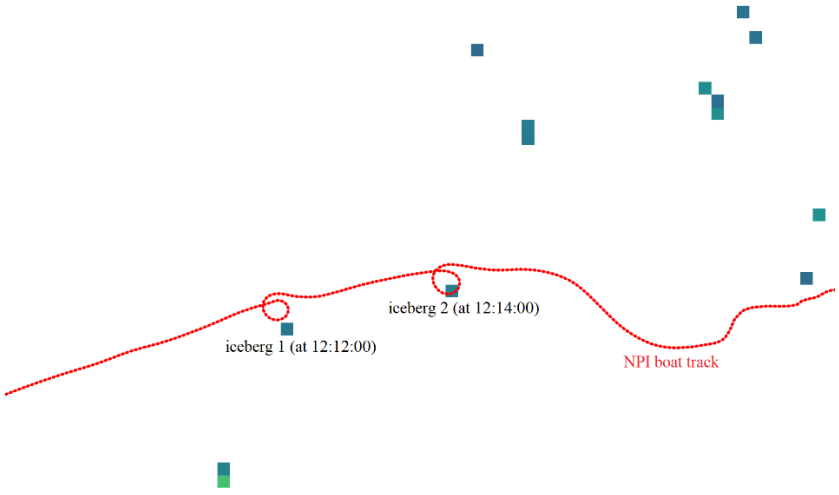

Figure 52: Focus on icebergs 1 and 2 including time of circumnavigation by the NPI boat (from 19.04.2018 12:15:01).

5 Discussion

At the beginning of this thesis, we formulated four essential research questions that are associated with my objectives.

1. Is it possible to identify icebergs in Kongsfjorden based on the backscatter intensity of the GPRI images?

It is definitely possible to detect icebergs based on GPRI backscatter images. The three examples in the previous chapter are showing that the GPRI is capable of detecting icebergs within the extent of our area of interest between Ny-Ålesund and Blomstrandhalvøya. In order to make a safe assumption about the GPRI's detection capabilities, we would have to investigate more examples. We could have collected more auxiliary datasets in addition to satellite SAR data, UAV images and boat track information. One option could be freely available passive Earth Observation imagery provided by ESA's Copernicus Programme.

2. Which threshold technique is the most adapted to the detection of icebergs based on GPRI images?

The best results can be obtained by applying the manual detection method. With the manual detection method, we can adjust the threshold until the most optimal threshold is assured. Unfortunately, the manual detection method has its flaws. The problem is that the relation between icebergs and background can vary from an image to another. For example, we could spend a long time analyzing six months of GPRI backscatter images taken every 15 min, because we have to set and adjust separately the threshold for each image. The manual detection method is clearly not feasible when it comes to big datasets.

The automated detection method has the disadvantage that it cannot detect as many icebergs as possible. The automated detection method at its current state is very basic and is based on empirical findings. For the next step, we could improve the automated detection method by applying single-feature-based detection algorithm. We are talking about a target detection method that has already been used in satellite SAR images. The idea is to code an algorithm in Python that allows us to utilize a sliding window based on a constant false alarm rate (CFAR) (figure 53). In the GPRI imagery case, the pixels under test (PUT) window should be one pixel small in order to detect even the smallest possible icebergs. The guard cells make sure that the pixels neighboring the PUT are not taken into consideration when comparing the PUT with the boundary ring window. The sliding window runs through the GPRI backscatter intensity images and is based on one- or multiple-parameter CFAR. For example, the sliding window ensures that we detect icebergs instead of noise by comparing the PUT with the boundary ring window. The automated detection algorithm can distinguish between an iceberg pixel and a large area of noise. Therefore, it is important to choose the correct sizing for the guard cells and the boundary ring window around the PUT. The guard cells window should have the size of the largest iceberg we could possibly detect in Kongsfjorden. The boundary ring window size should be chosen accordingly to the local sea clutter [23].

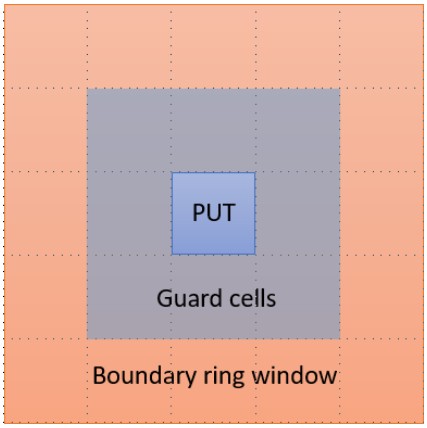

Figure 53: Sliding window for target detection.

3. Compared to complementary remote sensing and in-situ data, can we evaluate the quality of the results and identify false positives/negatives?

As already established and supported by complementary remote sensing and in-situ data, it is possible to detect icebergs in GPRI backscatter images. After conducting more validations with various auxiliary remote sensing data, we can make a final conclusion on how good the GPRI identifies icebergs in Kongsfjorden. In general, the detection performance is very high based on our validations with auxiliary data.

We could not find false positives in the georeferenced GPRI images from our examples in the thesis work. Probably, because of the effective manual detection method, we could avoid a lot of false positive detections. Furthermore, there were no false positive detections in the automated detection method. There is still a need to conduct research on the false positive rate in GPRI backscatter images.

4. What information, for example count, size or shape of icebergs, can we gain from the GPRI images?

We could successfully implement an algorithm that displays the basic information we can get about detected icebergs from the GPRI backscatter images. The basic parameters are position, count and size of the detected icebergs. The position of each iceberg represents its average x- and y-position in radar geometry after merging all neighboring pixels to one iceberg. The number of detected iceberg pixels in a GPRI backscatter image is represented by the parameter count. The size parameter simply equals the number of pixels each iceberg possesses. Implementing the iceberg parameter shape could not been implemented due to the limited time frame and complexity. Describing the shape of an iceberg in a GPRI backscatter image is depending on the backscatter intensity values of every single pixel belonging to an iceberg. From the backscatter intensity of a pixel, we can conclude the rough shape, for example high backscatter intensity most likely results in a large iceberg structure. Unfortunately, due to the randomness of iceberg structures and the resulting backscatter intensity, analyzing the parameter shape is hard to approach.

The next steps should be to implement a better positioning for icebergs in georeferenced GPRI images. In order to calculate the average position of one iceberg, evaluating the number and individual positions of all neighboring pixels belonging to this iceberg is necessary. The algorithm for the iceberg parameters, including the iceberg count, can be used in georeferenced

GPRI imagery. When using the algorithm of the thesis work for georeferenced GPRI images, it is necessary to change a few lines of code, for example for the input data we need georeferenced GPRI images instead of .slc products. An algorithm for iceberg positions in georeferenced GPRI images is beneficial for making more accurate validations with complementary remote sensing data, for example we could easily compare UAV images with icebergs. Knowing the position of both UAV and icebergs would enhance the validation process.

In addition to the iceberg parameters, we could implement an iceberg tracking algorithm based on every single iceberg's position. J. Olofsson has been developing a tracking system for drift ice based on satellite remote sensing data. J. Olofsson's is of particular use for iceberg tracking with GPRI backscatter imagery. The temporal resolution of 5 and 15 min of the GPRI data is a great benefit for developing the iceberg tracking algorithm, because the Multiple Hypothesis Tracking (MHT) would work more efficient. Basically, MHT includes the tracing of single targets in a cluster of data. It means that all new measurements are associated with either (1) the same target, (2) a completely new target or (3) simply an error. That means we compare every GPRI backscatter image with its following GPRI image and analyze how the iceberg positions change. The iceberg tracking system can give valuable insights into the currents in Kongsfjorden. But even without the tracking system, we can make conclusions on how much ice is floating in Kongsfjorden or calved from the tidewater glaciers. At the current state, we cannot give valuable information about the ice mass balance in Kongsfjorden [24].

In this thesis work, we just have been investigating the GPRI's detection capabilities at up to 4.1 km distance. We have to keep in mind that the GPRI's spatial resolution in azimuth direction is decreasing linearly with increasing distance. Which means that our validations might not be relevant anymore when we investigate beyond our area of interest. The worse performance in far range can influence the quality or even possibility of detecting icebergs in Kongsfjorden. However, a valuable future prospect would be to investigate the entire GPRI backscatter image instead of focusing on a small area of interest. One challenge would be to account for all the lagoons and coastal lines of Kongsfjorden, for example by masking them out in the GPRI backscatter images. The detrending processing has already been established successfully in this thesis work, which means that the linearly decreasing spatial resolution in azimuth direction will be the main concern in future works when it comes to investigations in the far range.

6 Conclusions

The GPRI is capable of detecting icebergs, but before analyzing the georeferenced GPRI images, we had to process the GPRI backscatter images. Detrending the entire used GPRI backscatter imagery is a necessity to account for the variation in backscatter intensity in range direction. After the detrending has eliminated the noise floor in range direction, we can proceed by choosing an area of interest in the GPRI backscatter image. Hereby, we avoid having lagoons and coastal lines within our area of interest. With no interfering structures, we can separate all icebergs in our area of interest from the surrounding sea. We are doing this by choosing one of two methods to set a threshold: the manual and automated detection method. The manual method proves to be the most effective one in setting the optimal threshold for distinguishing between icebergs and sea, but it is very inefficient to handle big amounts of data.

With further improvements, the automated detection method would become more effective than the manual detection method and it would not rely on empirical assumptions. After setting the most optimal threshold supported by histograms, we can collect the most important iceberg parameters, namely position, count and size. The georeferenced GPRI images got validated with complementary remote sensing data to investigate the GPRI's iceberg detection results. We had satellite SAR, UAV imagery and boat tracks to our disposal to make meaningful validations. Further, we can conclude that GPRI backscatter images have the potential of detecting icebergs and growlers at up to 4.1 km distance. The automated detection method and the iceberg parameter algorithm have the potential for improvements, which can be addressed in future projects. In addition, more validation examples should be conducted in order to make an adequate statement about the GPRI's iceberg detection performance. Nevertheless, our findings are promising and reveal the great potential of iceberg detection using the GPRI instrument. All in all, this thesis work laid the foundation for future iceberg detection research with the GPRI system in particular, but also ground-based radars in general.

References

[1] Climate Report Spitsbergen 2100: Concern and Many ... (n.d.). Retrieved February 10, 2019, from https://www.spitsbergen-svalbard.com/2019/02/08/climate-report-spitsbergen-2100-concern-and-many-questions.html

[2] Hop, H., Pearson, T., Hegseth, E. N., Kovacs, K. M., Wiencke, C., Kwasniewski, S., ... Gerland, S. (2006, December 14). The marine ecosystem of Kongsfjorden, Svalbard. Retrieved January 10, 2019, from http://onlinelibrary.wiley.com/doi/10.1111/j.1751-8369.2002.tb00073.x/abstract

[3] Hagen, J. O., Kohler, J., Melvold, K., & Winther, J. (2003). Glaciers in Svalbard: Mass balance, runoff and freshwater flux. *Polar Research, 22*(2), 145-159. doi:10.1111/j.1751-8369.2003.tb00104.x

[4] Dowdeswell, J. A., & Forsberg, C. F. (1992). The size and frequency of icebergs and bergy bits derived from tidewater glaciers in Kongsfjorden, northwest Spitsbergen. *Polar Research, 11*(2), 81-91. doi:10.3402/polar.v11i2.6719

[5] Turnbull, I. D., Fournier, N., Stolwijk, M., Fosnaes, T., & Mcgonigal, D. (2015). Operational iceberg drift forecasting in Northwest Greenland. *Cold Regions Science and Technology, 110*, 1-18. doi:10.1016/j.coldregions.2014.10.006

[6] Gerland, S., Winther, J., Ørbæk, J. B., & Ivanov, B. V. (1999). Physical properties, spectral reflectance and thickness development of first year fast ice in Kongsfjorden, Svalbard. *Polar Research, 18*(2), 275-282. doi:10.3402/polar.v18i2.6585

[7] Gerland, S., Haas, C., Nicolaus, M. and Winther, J. G. (2004): Seasonal development of structure and optical surface properties of fast ice in Kongsfjorden, Svalbard, Reports on Polar and Marine Research, 492, pp. 26-34. hdl:10013/epic.22392

[8] Gerland, S., & Hall, R. (2006). Variability of fast-ice thickness in Spitsbergen fjords. *Annals of Glaciology, 44*, 231-239. doi:10.3189/172756406781811367

[9] Akbari, V., & Brekke, C. (2017). Iceberg detection in open water and sea ice using C-band radar polarimetry. *2017 IEEE International Geoscience and Remote Sensing Symposium (IGARSS)*. doi:10.1109/igarss.2017.8127449

[10] Ulaby, F., & Long, D. (2014). Microwave Radar and Radiometric Remote Sensing. doi:10.3998/0472119356

[11] Escalante-Ramírez, B. (2012). *Remote sensing: Applications*. Rijeka: InTech.

[12] Voytenko, D., Dixon, T. H., Luther, M. E., Lembke, C., Howat, I. M., & Peña, S. D. (2015). Observations of inertial currents in a lagoon in southeastern Iceland using terrestrial radar interferometry and automated iceberg tracking. *Computers & Geosciences, 82*, 23-30. doi:10.1016/j.cageo.2015.05.012

[13] Voytenko, D., Dixon, T. H., Howat, I. M., Gourmelen, N., Lembke, C., Werner, C. L., . . . Oddsson, B. (2015). Multi-year observations of Breiðamerkurjökull, a marine-terminating glacier in southeastern Iceland, using terrestrial radar interferometry. *Journal of Glaciology, 61*(225), 42-54. doi:10.3189/2015jog14j099

[14] Gerland, S., & Renner, A. H. (2007). Sea-ice mass-balance monitoring in an Arctic fjord. *Annals of Glaciology, 46*, 435-442. doi:10.3189/172756407782871215

[15] Caduff, R., Schlunegger, F., Kos, A., & Wiesmann, A. (2014). A review of terrestrial radar interferometry for measuring surface change in the geosciences. *Earth Surface Processes and Landforms, 40*(2), 208-228. doi:10.1002/esp.3656

[16] Werner, C., Strozzi, T., Wiesmann, A., & Wegmüller, U. (n.d.). Gammas portable radar interferometer | Request PDF. Retrieved January 16, 2019, from https://www.researchgate.net/publication/253700589_Gammas_portable_radar_interferometer

[17] The GPRI multi-mode differential interferometric radar for ... (n.d.). Retrieved January 16, 2019, from https://www.researchgate.net/publication/260122330_The_GPRI_multi-mode_differential_interferometric_radar_for_ground-based_observations

[18] Werner, C., Strozzi, T., Wiesmann, A., & Wegmüller, U. (n.d.). (PDF) A Real-Aperture Radar for Ground-Based Differential ... Retrieved January 16, 2019, from https://www.researchgate.net/publication/224383362_A_Real-Aperture_Radar_for_Ground-Based_Differential_Interferometry

[19] Ulaby, F., & Long, D. (2014). Microwave Radar and Radiometric Remote Sensing. doi:10.3998/0472119356

[20] Gill, R. (2001). Operational Detection of Sea Ice Edges and Icebergs Using SAR. *Canadian Journal of Remote Sensing, 27*(5), 411-432. doi:10.1080/07038992.2001.10854884

[21] Denbina, M., & Collins, M. J. (2012). Iceberg Detection Using Compact Polarimetric Synthetic Aperture Radar. *Atmosphere-Ocean, 50*(4), 437-446. doi:10.1080/07055900.2012.733307

[22] Sivertsen, Borch, Arntzen, & R., T. (2018, December 01). Real-time and Autonomous Detection of Sea Ice and Growlers Using UAS. Retrieved April 21, 2019, from http://adsabs.harvard.edu/abs/2018AGUFM.C31E1578S

[23] El-Darymli, Khalid, et al. "Errata: Target Detection in Synthetic Aperture Radar Imagery: a State-of-the-Art Survey." *Journal of Applied Remote Sensing*, vol. 7, no. 1, 2013, p. 079998., doi:10.1117/1.jrs.7.079998.

[24] Olofsson, J., Brekke, E., Fossen, T. I., & Johansen, T. A. (2017). Spatially indexed clustering for scalable tracking of remotely sensed drift ice. *2017 IEEE Aerospace Conference,* 1-13. doi:10.1109/aero.2017.7943670

Appendix

Iceberg detection code (from the file iceberg_detection.py):

```
import sys
import scipy as sp
import scipy.interpolate
import numpy as np
from matplotlib import pyplot as plt
import gdar
import gdarplus
from gdarplus import gbradar
from gdar import const
from gdar.rastertools import downsample
from gdar import util
from gdar import gtime
import gdar.fileformats
import gdarplus.geocode as geocode

#++++++++++++++++++++++++++ICEBERG DETECTION++++++++++++++++++++++++++++++++++++
#+++++++++++++++++++++++++++STEP01++++++++++++++++++++++++++++++++++++++++++++
        #Reading GPRI image in radar geometry
        #Getting new more precise heading
ref_lat = 78.945940
ref_lon = 11.874863
ref_ypos = 57

im = '/rawdata/gbradar/GPRI2/Kongsfjorden_2018/5_min/20180420/20180420_194501u.slc'

        #Reading upper collection
usrc = gbradar.reader(im)
heading = gbradar.heading_from_ref(usrc, ref_ypos, (ref_lat, ref_lon))
itmp = gbradar.adjust_heading(usrc, heading=heading)
        #azimuth multilooking
dx = 6
        #range
dy = 8
        #logabs: on dB scale
dr = downsample(itmp, (dx, dy), average='logabs')
#+++++++++++++++++++++++++++++++++++++++++++++++++++++++++++++++++++++++++++++


#+++++++++++++++++++++++++++++STEP02++++++++++++++++++++++++++++++++++++++++++
        #Detrending to remove the variation in backscatter intensity
        #in range direction

        #to even out image from gbradar data
        #for radar geometry: backscatter compensation for range
        #it needs .npz file
        #Stored in the file:    - range times (rtime)
        #                       - corresponding backscatter correction value for those range times (correction)
        #How to?    - averaging the backscatter for azimuth lines 10-60 to form one line (in range) for an image
        #           - calculating this line for all images in the 5 min data folder
        #           - averaging all these lines to form the line stored in the .npz file
rlen = dr.shape[1]
rng = np.load('range_profile.npz')

idxs = dr.idx_from_coord((np.zeros(rlen), rng['rtime']))

        #fill_value: Value to use outside of the area given in rng['rtime']
        #If requesting a value below np.min(rng['rtime']) or above np.max(rng['rtime']), will return this fill value
        #probably removing fill_value (gives bad results for values above max)
        # , fill_value = 0.02 * 3.6)
fit = scipy.interpolate.interpld(idxs[1], rng['correction'], bounds_error = False)(np.arange(rlen))

        #to form an array: scale takes the vector "fit" (of lenght rlen) and repeats it dr.shape[1] times
scale = (np.ones(dr.shape[0])[:, np.newaxis] * fit[np.newaxis, :])
sig = dr[:, :]
        #remove the increase in range on the backscatter for thresholding algorithm
        #for linear scale:
# sig_corrected = sig/scale
        #but data out of downsample is on dB scale
        #for dB scale:
sig_corrected = sig - np.log10(np.abs(scale))

        #plotting original data raster (dr)
plt.figure('STEP01 dr')
plt.clf()
plt.imshow(dr[:,:])
plt.title('GPRI original backscatter image in radar geometry')
plt.xlabel('Range direction')
plt.ylabel('Azimuth direction')
plt.axis([0, 2804, 0, 141])
clb = plt.colorbar()
clb.ax.set_title('backscatter intensity in dB')
```

```
        #plotting corrected data raster (sig_corrected)
plt.figure('STEP02 sig_corrected')
plt.clf()
plt.imshow(sig_corrected[:,:])
plt.title('GPRI corrected backscatter image in radar geometry')
plt.xlabel('Range direction')
plt.ylabel('Azimuth direction')
plt.axis([0, 2804, 0, 141])
clb = plt.colorbar()
clb.ax.set_title('backscatter intensity in dB')

        #corrected dataraster
        #converting sig_corrected array into dataraster dr_corrected
        #converting numpy array back to data raster
        #(np to dr)
        #(meta is for the area [0:141, 0:2804])
corrected_meta = gdar.rastertools.view(dr, (120,700), (15,200)).meta
        #(data is for the area [15:120, 200:700])
dr_corrected = gdar.raster.DataRaster(sig_corrected[15:120, 200:700], corrected_meta)
#++++++++++++++++++++++++++++++++++++++++++++++++++++++++++++++++++++++++++++++++++++


#++++++++++++++++++++++++++++++STEP03++++++++++++++++++++++++++++++++++++++++++++++
        #Selecting area of interest

ysize = 120; xsize = 700; ystart = 0; xstart = 0
        #conversion from data raster to numpy array (for area of interest (aoi))
        #(dr to np)
        #but in case it is a tuple:
        #np.asarray(..._from_idx((np.arange(..., ...),np.arange(..., ...)),grid=True))
        #meta and data need to come from the same pixels
        #(= same start point and same size)
aoi = gdar.rastertools.view(dr_corrected, (ysize,xsize), (ystart,xstart))[:,:]

        #plotting area of interest
plt.figure('STEP03 area of interest')
plt.clf()
plt.imshow(aoi)
plt.title('GPRI backscatter image within area of interest in radar geometry')
plt.xlabel('Range direction')
plt.ylabel('Azimuth direction')
plt.axis([0, 2804, 0, 141])
clb = plt.colorbar()
clb.ax.set_title('backscatter intensity in dB')
#++++++++++++++++++++++++++++++++++++++++++++++++++++++++++++++++++++++++++++++++++++

#++++++++++++++++++++++++++++++STEP04++++++++++++++++++++++++++++++++++++++++++++++
        #Checking the distribution of backscatter values

        #plotting the histogram
plt.figure('STEP04 histogram aoi #1')
plt.clf()
histval, loc = np.histogram(aoi, bins = 200)
plt.plot(loc[:-1], histval)
plt.title('Histogram for pixels within area of interest')
plt.xlabel('Backscatter intensity values')
plt.ylabel('Pixel count')

plt.figure('STEP04 histogram aoi #2')
plt.clf()
plt.hist(aoi, histtype='bar', bins = None)
plt.title('Histogram for pixels within area of interest')
plt.xlabel('Backscatter intensity values')
plt.ylabel('Pixel count')
#++++++++++++++++++++++++++++++++++++++++++++++++++++++++++++++++++++++++++++++++++++


#++++++++++++++++++++++++++++++STEP05++++++++++++++++++++++++++++++++++++++++++++++
        #Testing different thresholds

        #finding manually the percentile value (for thresholds)
        #when the desired percentile lies between two data points
        #nearest interpolation
        #working with the remaining % of the values
        #(which are most likely bergy bits)
        # value best compromise between rough and calm sea
# percentile = np.percentile(aoi, 99.88, interpolation='nearest')

        #threshold for the subset
        #separating icebergs from the water
# thresh = aoi[:,:]
        #to avoid: "RuntimeWarning: invalid value encountered in less/greater"
# np.warnings.filterwarnings('ignore')
        #set the threshold to an empirical value (not anymore!)
        #now: taking the percentile value from above
# thresh[thresh < percentile ] = None

        #manual threshold
thresh = aoi[:,:]
thresh[thresh < -0.8] = None
```

```
        #plotting the threshold image for the corrected area of interest
plt.figure('STEP05 threshold')
plt.clf()
plt.imshow(thresh)
plt.title('Area of interest and potential iceberg targets in radar geometry')
plt.xlabel('Range direction')
plt.ylabel('Azimuth direction')
plt.axis([0, 2804, 0, 141])
clb = plt.colorbar()
clb.ax.set_title('backscatter intensity in dB')
#++++++++++++++++++++++++++++++++++++++++++++++++++++++++++++++++++++++++++++++++++++


#++++++++++++++++++++++++++++++STEP06++++++++++++++++++++++++++++++++++++++++++++++
        #Again:
        #Checking the distribution of backscatter values
        #for potential icebergs vs sea

# only_icebergs = thresh[:,:]
# only_icebergs[np.isnan(only_icebergs)] = -10

        #claculating XXth percentile (declared above) while ignoring NaNs
# print('XXth percentile: ', np.nanpercentile(thresh, 99.88, interpolation='nearest'))
        #claculating median (50th percentile) while ignoring NaNs
# med = np.nanmedian(only_icebergs)
# print('Median: ', med)
        #compute standard deviation while ignoring NaNs
# std = np.nanstd(only_icebergs, dtype=np.float64)
# print('Standard deviation: ', std)

        #plotting the histogram
# plt.figure('STEP06 next histogram aoi #1')
# plt.clf()
# # plt.hist(aoi, histtype='bar')
# histval, loc = np.histogram(aoi, bins = 200)
# plt.plot(loc[:-1], histval)
# plt.title('Histogram for iceberg pixels within area of interest')
# plt.xlabel('Backscatter intensity values')
# plt.ylabel('Pixel count')

# plt.figure('STEP06 next histogram aoi #2')
# plt.clf()
# plt.hist(only_icebergs, histtype='bar', bins = None, range=(-2, 2))
# plt.title('Histogram for iceberg pixels within area of interest')
# plt.xlabel('Backscatter intensity values')
# plt.ylabel('Pixel count')


# thresh[thresh < med ] = None
# new_med = np.nanmedian(only_icebergs)
# print('New Median: ', new_med)
# new_std = np.nanstd(thresh, dtype=np.float64)
# print('New Standard deviation: ', new_std)

    #plotting the threshold image for the corrected area of interest
# plt.figure('STEP06 new threshold (median)')
# plt.clf()
# plt.imshow(thresh)
# plt.axis('equal')
# plt.colorbar()
# plt.title('Area of interest and final threshold in radar geometry')
# plt.xlabel('Range direction')
# plt.ylabel('Azimuth direction')
#++++++++++++++++++++++++++++++++++++++++++++++++++++++++++++++++++++++++++++++++++++


#++++++++++++++++++++++++++++++STEP07++++++++++++++++++++++++++++++++++++++++++++++
        #checking the resulting final dataraster
        #before georeferencing the results
        #detected icebergs

        #merging final threshold with the dataraster dr_corrected
merge = dr_corrected[:,:]
merge[ystart:ystart+ysize,xstart:xstart+xsize] = thresh
dr_final = gdar.raster.DataRaster(merge, dr_corrected.meta)

dr_subplot = gdar.raster.DataRaster(thresh, dr_corrected.meta)

        #plotting dr_final (= original dr + dr_iceberg)
# plt.figure('STEP07 dr_final')
# plt.clf()
# plt.imshow(dr_final[:,:])
# plt.axis('equal')
# plt.colorbar()
# plt.title('Final data raster including the area of interest')
# plt.xlabel('Range direction')
# plt.ylabel('Azimuth direction')

        #final datarater in polar projection
aa = dr_final[40:80,400:600]

azix = np.arange(dr_final.shape[0]+1)-0.5
rgix = np.arange(dr_final.shape[1]+1)-0.5
azc, rgc = dr_final.coord_from_idx((azix, rgix))
```

```
th = np.radians(90-azc)
xx = const.c/2 * rgc * np.cos(th)[:,None]
yy = const.c/2 * rgc * np.sin(th)[:,None]
dd = 10 * dr_final[:,:]

        #plotting dd in polar coordinates
# plt.figure('dd')
# plt.clf()
# plt.pcolormesh(xx, yy, dd, vmin = -20, vmax = 5)
# plt.axis('equal')
# plt.title('GPRI backscatter image in polar coordinates')
# clb = plt.colorbar()
# clb.ax.set_title('backscatter intensity in dB')
#++++++++++++++++++++++++++++++++++++++++++++++++++++++++++++++++++++++++++++++++

plt.show()

#++++++++++++++++++++++++++++++STEP09++++++++++++++++++++++++++++++++++++++++++++
        #geo-referencing
# import gdarplus.geocode as geocode
# import gdar.fileformats
# import metatools
# import gdarplus.earth

        #area of interest
path = 'GPRI_geoc_final_evaluation/20180420_194501_aoi_auto.tif'
demfile = '/rawdata/auxdata/dem/Svalbard/s100dtm20.tif'
#demdr = gdarplus.earth.add_geoid_height(gdar.fileformats.read_crs(demfile))
demdr = geocode.add_geoid_height(gdar.fileformats.read_crs(demfile))
gcod = geocode.geocoding(dr_final, demdr, fullrd=True, out_type=None, order=0)
#gcod = geocode.geocoding(dr_corrected, demdr, fullrd=True, out_type=None, order=0)
gdar.fileformats.write_crs(gcod, path)

        #area [0:141, 0:2804]
corrected_meta2 = gdar.rastertools.view(dr, (141,2804), (0,0)).meta
dr_corrected2 = gdar.raster.DataRaster(sig_corrected[0:141, 0:2804], corrected_meta2)

path = 'GPRI_geoc_final_evaluation/20180420_194501_all_auto.tif'
demfile = '/rawdata/auxdata/dem/Svalbard/s100dtm20.tif'
demdr = geocode.add_geoid_height(gdar.fileformats.read_crs(demfile))
gcod = geocode.geocoding(dr_corrected2, demdr, fullrd=True, out_type=None, order=0)
gdar.fileformats.write_crs(gcod, path)

# gdar.fileformats.write_gdr(dr_corrected, 'final_geocode.gdar')
#++++++++++++++++++++++++++++++++++++++++++++++++++++++++++++++++++++++++++++++++


#+++++++++++++++Iceberg parameters++++++++++++++++++++++++++++++++++++++++++++++
class Pixel:
    def __init__(self, x, y, intensity):
        self.x = x
        self.y = y
        self.intensity = intensity
        #initially -1 to show it is not stored in any iceberg
        self.iceberg_index = -1

        #function which changes the index to anything needed
        #iceberg index contained in a pixel is ...
        #... used to place neighbouring pixels in the same iceberg-object
    def update_iceberg_index(self, idx):
        self.iceberg_index = idx

class Iceberg:
        #list of pixels (which are neighbours) and also a size of the list
    def __init__(self):
        self.pixels = []
        self.size = 0

        #function adds a new pixel to the list and increases the size
    def append(self, pixel):
        self.pixels.append(pixel)
        self.size += 1

        #after the entire iceberg gets all its pixels appended ...
        #... calculating the average position of the iceberg from all pixel values
    def calculate_average_position(self):
        x_sum = 0
        y_sum = 0

        for pixel in self.pixels:
            x_sum += pixel.x
            y_sum += pixel.y

        #finding the average position by dividing by the length of the list of pixels
        #(the number of pixels contained in the iceberg)
        x_sum /= len(self.pixels)
        y_sum /= len(self.pixels)

        return (x_sum, y_sum)

        #to keep track of all entries in the array that is actually pixels
iceberg_list = []
```

```
        #updated version: without so many if statements
def is_neighbours(x1, y1, x2, y2):
    if(abs((x1 - x2) + (y1 - y2)) == 1):
        return True
    # elif(abs((x1 - x2) + (y1 - y2)) == 2):
    #     return True
    else:
        return False

        #to keep track of every iceberg
pixel_list = []

x = 0
y = 0

        #extend of the 2D array
array_max_x = 500
array_max_y = 105

        #in x-direction
for x in range(0, array_max_x):

        #in y-direction
    for y in range(0, array_max_y):

        #checking if entry is pixel or NaN
        if(np.isfinite(thresh[y,x])):
        #find the intensity of the pixel
            intensity = thresh[y,x]

        #creating a pixel object based on Pixel class
            pixel = Pixel(x, y, intensity)

        #append it to the list of pixels
            pixel_list.append(pixel)

        #registering all the pixels only one time
        #making sure none of them get put in different icebergs
        #for every pixel in the pixel list
for pixel1 in pixel_list:
        #for every other pixel in the list
    for pixel2 in pixel_list:
        #if the pixel has not been added to a list: creating a new iceberg object
        #... and append it to the list
        if(pixel1.iceberg_index == -1):
            iceberg = Iceberg()
            iceberg.append(pixel1)


        #changing the iceberg-index of the pixel
            pixel1.update_iceberg_index(len(iceberg_list))

        #then append the pixel itself to the list
            iceberg_list.append(iceberg)

        #if the pixels are not the same and they are neighbours
        if(pixel1 != pixel2) and is_neighbours(pixel1.x, pixel1.y, pixel2.x, pixel2.y and pixel2.iceberg_index == -1):
        #append pixel2 to the same list as pixel1
        #then change the index of pixel2
        #making sure that it is located in the same list as pixel1
            iceberg_list[pixel1.iceberg_index].append(pixel2)
            pixel2.update_iceberg_index(pixel1.iceberg_index)

print("...")
print("Pixel count: ", len(pixel_list))
print("Iceberg count: ", len(iceberg_list))
print("Shape of aoi: ", thresh.shape)
print("...")

        #printing information
        #iterating over the list with a loop
index_i = 0
for iceberg in iceberg_list:
    print("Iceberg number: ", index_i, ".. Size: ", iceberg.size, ".. Average position: ", iceberg.calculate_average_position())
    index_i += 1
#++++++++++++++++++++++++++++++++++++++++++++++++++++++++++++++++++++++++++++++++++++
```